Title
Elucidating Molecular Mechanisms of Iron-Sulfur Protein Maturation Mediated by the Cytosolic Iron-Sulfur Cluster Assembly Pathway

Author
Fan, Xiaorui

Publication Date
2022

Peer reviewed|Thesis/dissertation

UNIVERSITY OF CALIFORNIA

Los Angeles

Elucidating Molecular Mechanisms of Iron-Sulfur Protein Maturation Mediated by the Cytosolic Iron-Sulfur Cluster Assembly Pathway

A dissertation submitted in partial satisfaction of the requirements

for the degree Doctor of Philosophy in Molecular Biology

by

Xiaorui Fan

2022

ABSTRACT OF THE DISSERTATION

Elucidating Molecular Mechanisms of Iron-Sulfur Protein Maturation Mediated by the Cytosolic Iron-Sulfur Cluster Assembly Pathway

by

Xiaorui Fan

Doctor of Philosophy in Molecular Biology

University of California, Los Angeles, 2022

Professor James Akira Wohlschlegel, Chair

Iron-sulfur (Fe-S) proteins are proteins containing the omnipresent Fe-S clusters as cofactors. Studies have accumulated demonstrating that Fe-S proteins are involved in a plethora of essential cellular functions. In eukaryotes, the cytosolic iron-sulfur cluster assembly (CIA) pathway, which depends on the mitochondrial iron-sulfur cluster assembly (ISC) pathway, facilitates Fe-S cluster incorporation into extramitochondrial Fe-S proteins. These include nuclear proteins required for DNA replication and DNA damage repair, as well as cytosolic proteins required for maintaining cellular iron homeostasis and ribosomal functions. In the CIA pathway, [4Fe-4S] cluster are assembled on the CIA scaffold complex, transferred to CIAO3, and incorporated into CIA substrates via the CIA targeting complex. The maturation of CIA substrates is controlled by cellular iron and oxygen. We demonstrate in this study that the incorporation of CIAO3 into CIA machineries is iron regulated, which may account for

this precise control of substrate maturation. We developed a targeted proteomics assay to monitor the presence and abundance of known CIA components and prototypical substrates. Using this assay, we were able to detect that the CIA targeting complex and CIA substrates associated with NUBP2, a component of the CIA scaffold complex. This suggests the possible formation of higher order meta complexes composed of the CIA scaffold complex, CIAO3, the CIA targeting complex and CIA substrates. We show that the interaction between CIAO3 and the CIA scaffold complex is affected by cellular iron availability, and this interaction is additionally strengthened under hypoxic environments and weakened by reactive oxygen species. Furthermore, we found that CIAO3 integration into CIA machineries demands a functional ISC pathway. Moreover, we generated CIAO3 mutants defective in Fe-S cluster binding and observed reduced interactions with both the CIA scaffold complex and the CIA targeting complex. However, stronger interactions with substrates were observed in these mutants, suggesting that CIAO3 and CIA substrates may be present in complexes in the absence of the CIA targeting complex. Lastly, we revealed that the CIAO3 mutant that associates with pulmonary arteriovenous malformations is incapable of integrating into the CIA machineries, which may partially explain the pathological outcome of this mutation. Together, these findings demonstrate the reorganization of the CIA machinery in different cellular environments. Alongside this, we investigated the architecture of the CIA targeting complex with crosslinking mass spectrometry and found that CIAO2B is in contact with the C-terminus of MMS19. A CIA substrate, CDKAL1, is also in close proximity to the C-terminus of MMS19.

The dissertation of Xiaorui Fan is approved.

Elizabeta Nemeth

Feng Guo

Joseph Ambrose Loo

Keriann Marie Backus

James Akira Wohlschlegel, Committee Chair

University of California, Los Angeles

2022

TABLE OF CONTENTS

LIST OF FIGURES

LIST OF TABLES

ACKNOWLEDGEMENT

First of all, I would love to thank my mother, my grandparents and my husband. Pursuing science is a challenging journey and I would not have been able to reach this point of education without their unconditional love and support.

I am also extremely grateful for the help I received from my thesis committee members over the course of my study. Dr. Elizabeta Nemeth, Dr. Feng Guo, Dr. Joseph Loo and Dr. Keriann Backus have offered me insightful scientific inputs that greatly enhanced my projects and valuable suggestions on career development.

I would like to further extend my acknowledgement to members of the Wohlschlegel lab. I have benefited from the knowledge of Dr. William Barshop and Dr. Ajay Vashisht in both proteomics and iron-sulfur cluster biogenesis. In addition, William optimized the instrument setup for data-dependent acquisition, which was used throughout this thesis. Ajay performed a lot of pilot experiments that accelerated the development of my projects. I would also like to thank Dr. Michele Bianchi whom I worked together with to optimize the workflow for crosslinking mass spectrometry. I was also very lucky to mentor Stephanie Leal, a very talented undergraduate student who helped me with validating the interactome of the CIA scaffold complex. Joining the lab together with Dr. Vijaya Pandey and Shima Rayatpisheh was such a pleasant experience, and I have had inspiring conversations with them both inside and beyond science. I would also like to thank Dr. Yasaman Jami and Jihui Sha for keeping our precious Fusion Lumos in good shape. Dr. Adarsh Mayank, Dr. Brian Young, Weixian Deng, Hee Jong Kim, Tanu Sharma and Dr. David Powers are wonderful colleagues, and I am thankful to work beside them during my study in the Wohlschlegel lab.

Moreover, I want to express my appreciation to all my mentors throughout my academic trainings, for guiding me with their knowledge and inspiring me with their passion for science. I would also like to thank Dr. Steven Clarke, for directing the Cellular and Molecular Biology Training Program and creating a communicative learning environment. Additionally, I would like to acknowledge the efforts of the administrative personnel in Molecular Biology Interdepartmental Doctoral Program and Department of Biological Chemistry.

To my dearest friends, I want to thank you all for sharing the joyful moments in this journey and understanding my frustrations. It is your company that made me strong.

Lastly, I would love to express my deepest gratitude to Dr. James Wohlschlegel for being my thesis advisor. James provided me with his expert advice on developing these projects. More importantly, he gave me the opportunity to work on these projects from the beginning, freely explore new directions, think independently and grow as a scientist. I feel incredibly fortunate to have his guidance and support over the past six years.

My dissertation was partially funded by the Graduate Dean's Scholar Award, the Cellular and Molecular Biology Training Grant (Ruth L. Kirschstein National Research Service Award GM007185) and the Philip Whitcome Pre-doctoral Fellowship.

Chapter 2 is currently accepted at *Journal of Biological Chemistry.*

VITA

EDUCATION

2022 **Ph.D. Candidate, Molecular Biology**

Thesis: Elucidating Molecular Mechanisms of Iron-Sulfur Protein Maturation Mediated by the Cytosolic Iron-Sulfur Cluster Assembly (CIA) Pathway

University of California - Los Angeles, Los Angeles, California

2014 **M.S., Chemistry and Biochemistry**

University of California - San Diego, La Jolla, California

2011 **B.S., Chemistry (Honors Curriculum in Chemistry Research)**

Minor: Biology

Thesis: The Water Effect on the OH Reaction with Methanol

Purdue University, West Lafayette, Indiana

SCHOLARSHIPS, GRANTS AND AWARDS

2020 **Keystone Symposia Scholarship**

2019-2020 **The Philip Whitcome Pre-doctoral Fellowship**

Molecular Biology Institute, University of California, Los Angeles

2016-2018 **Cellular and Molecular Biology Training Grant**

Ruth L. Kirschstein National Research Service Award GM007185

University of California, Los Angeles

2015-2017 **Graduate Dean's Scholar Award**

University of California, Los Angeles

PUBLICATIONS

Fan X, Barshop WD, Vashisht AA, Pandey V, Leal S, Rayatpisheh S, Jami-Alahmadi Y, Sha J, Wohlschlegel JA (2022). Iron-Regulated Assembly of the Cytosolic Iron-Sulfur Cluster Biogenesis Machinery. *J Biol Chem*. DOI: 10.1016/j.jbc.2022.102094.

Grolla AA, Miggiano R, Daniele Di Marino, Bianchi M, Gori A, Orsomando G, Gaudino F, Galli U, Erika Del Grosso, Mazzola F, Angeletti C, Guarneri M, Torretta S, Calabrò M, Boumya S, **Fan X**, Colombo G, Travelli C, Rocchio F, Aronica E, Wohlschlegel JA, Deaglio S, Rizzi M, Genazzani AA and Garavaglia S (2020). A Nicotinamide phosphoribosyltransferase-GAPDH Interaction Sustains the Stress-Induced NMN/NAD+ Salvage Pathway in the Nucleus. *J Biol Chem*, DOI:10.1074/jbc.RA119.010571.

Barshop WD, Kim HJ, **Fan X**, Sha J, Rayatpisheh S, Wohlschlegel JA. (2019). Chemical Derivatization of Affinity Matrices Provides Protection from Tryptic Proteolysis. *J Proteome Res*, 18(10), 3586-3596.

PRESENTATIONS

Fan X, Barshop WD, Vashisht AA, Wohlschlegel JA. (2021, October). Dynamic Assembly of the Cytosolic Iron-Sulfur Cluster Biogenesis Machinery Regulated by Iron-Sulfur Cluster Incorporation of CIAO3. Poster presented at Gordon Research Conference and Gordon Research Seminar: Cell Biology of Metals

Fan X, Barshop WD, Vashisht AA, Wohlschlegel JA. (2020, September). Elucidating the Molecular Regulation of Cytosolic Iron-Sulfur Cluster Biogenesis. Poster presented at Keystone eSymposia: Proteomics in Cell Biology and Disease.

CHAPTER 1

INTRODUCTION

Iron-Sulfur Clusters in Proteins

Iron-sulfur (Fe-S) clusters are inorganic cofactors ubiquitous in all realms of life. These cluster can present in multiple forms resulting from different oxidation states and stoichiometries of iron and sulfur, with [2Fe-2S], [3Fe-4S] and [4Fe-4S] clusters most commonly seen in biological systems.[1,2] Given the chemical versatility, Fe-S clusters typically serve as redox centers. Fe-S clusters are broadly known for facilitating the electron transfer in oxidative phosphorylation.[3] In addition, studies have suggested that Fe-S clusters in proteins serve as electron donors and acceptors in DNA mediated charge transfer.[4] The redox property of Fe-S clusters is also necessary for binding and activation of substrates in enzymes such as aconitase, hydrogenase and reductase.[1] Aside from being redox centers, Fe-S clusters also play structural roles in Fe-S proteins. Loss of Fe-S clusters due to either mutations at cluster binding sites or impaired Fe-S cluster biogenesis often compromises the structural integrity of Fe-S proteins.[5,6]

The emerging role of Fe-S clusters has been well recognized in sensing changes in cellular environments. Upon environmental stimuli, the diversity and chemical versatility of Fe-S clusters allow them to convert between different forms, subsequentially altering protein activities. Below are three examples of cluster conversions induced by environmental stimuli:

(1) $[4Fe\text{-}4S]^{2+} \leftrightarrow [3Fe\text{-}4S]^{1+} + Fe^{2+} + e^-$

(2) $[4Fe\text{-}4S]^{2+} + O_2 \rightarrow [2Fe\text{-}2S]^{2+}$

(3) $[2Fe\text{-}2S]^{1+}$ + superoxide/NO $\rightarrow [2Fe\text{-}2S]^{2+}$

Iron regulatory protein 1 (IRP1) has dual functions that the apo-IRP1 binds iron-responsive elements (IREs) to regulate cellular iron homeostasis while the Fe-S cluster

bound IRP1 serves as the cytosolic aconitase.[7] The active IRP1 contains a [4Fe-4S] cluster, which undergoes a reversible conversion through reaction (1) upon iron starvation or oxidation, leading to IRP1 inactivation.[7,8] However, this [3Fe-4S] cluster bound IRP1, although inactive, does not bind IREs until the cluster is further degraded. Reaction (2) was observed in the regulation of bacteria fumarate and nitrate reduction regulatory protein (FNR).[9] Under anaerobic conditions, FNR exists in a dimeric form containing [4Fe-4S] clusters and triggers the transcription of genes needed for anaerobic growth. When bacteria are exposed to oxygen, the cluster conversion in reaction (2) leads to the dissociation of dimeric FNR and reduces its DNA binding. Reaction (3) was observed in the activation of the redox-sensitive transcriptional activator SoxR. With exposure to superoxide or NO, oxidation of the inactive SoxR promotes the transcription of SoxS that controls the expression of genes for superoxide removal. These examples of cluster conversion in IRP1, FNR and SoxR illustrate that Fe-S clusters provide an additional layer of protein regulation in response to changes in intracellular iron level, oxygen concentration and reactive oxygen species.

There are over 160 proteins known to contain Fe-S clusters, and the number is still growing.[1] In human proteome, 0.35% are predicted to be Fe-S proteins.[10] The functions of Fe-S proteins have expanded from electron transport to DNA replication, transcription, translation and a number of other functions yet to mention. Regardless of the widespread use of Fe-S clusters, their biogenesis is tightly regulated.

Biogenesis of Iron-Sulfur Clusters

The Fe-S cluster biogenesis in bacteria is mainly carried out by two pathways: ISC and SUF.[11] Under normal conditions, the clusters are assembled and transferred

into apo recipient proteins through the ISC pathway. Under conditions such as iron depletion or oxidative stress, the SUF pathway takes over the task of Fe-S cluster biogenesis. In eukaryotes where the cellular contents are compartmentalized, the biogenesis of Fe-S clusters is also compartmentalized.[12] The mitochondrial iron-sulfur cluster assembly (ISC) pathway, which is adapted from the bacterial ISC, mediates the cluster insertion into mitochondrial Fe-S proteins. Meanwhile, the cytosolic iron-sulfur cluster assembly (CIA) pathway, which depends on the function of the ISC pathway, facilitates cluster transfer into extramitochondrial Fe-S proteins.

The biogenesis of Fe-S clusters in the eukaryotic ISC pathway starts with the *de novo* [2Fe-2S] cluster assembly on the scaffold complex that consists of ISCU.[13,14] This step requires sulfides, irons, and electrons: sulfides are provided by the cysteine desulfurase NFS1, electrons are provided by the ferredoxin FDX1; frataxin, FXN, possibly provides irons for the cluster assembly. The cluster assembled is then transferred to monothiol glutaredoxin GLRX5 and is either directly inserted into [2Fe-2S] substrates or transferred for [4Fe-4S] cluster assembly on the complex composed of ISCA1, ISCA2 and IBA57. Insertion of [4Fe-4S] cluster into substrates is mediated by substrate specific targeting proteins.

The CIA pathway, which is parallel to the ISC pathway, facilitates Fe-S cluster incorporation into extramitochondrial Fe-S proteins (Fig. 1). [2Fe-2S] clusters are assembled on the complex composed of BOLA2 and GLRX3, with the iron chaperone protein PCBP1 interacting with BOLA2 to deliver iron from the labile iron pool (LIP).[15] [2Fe-2S] clusters are required for the maturation of CIAPIN1, which mediates the electron transfer from NADPH to the CIA scaffold complex composed of NUBP1 and

NUBP2, where [4Fe-4S] clusters are assembled.[16,17] The clusters are then transferred to a cluster carrier protein CIAO3, and eventually incorporated into the CIA substrates through the activity of the CIA targeting complex composed of MMS19, CIAO1 and CIAO2B.[5,18,19] CIAO2A, a homolog of CIAO2B, binds to CIAO1 but not MMS19.[20] It is suggested that CIAO2A may be responsible for maturation of a different set of substrates. Substrates targeted by the CIA pathway are involved in a plethora of essential cellular functions. As a result, the malfunction of the Fe-S cluster assembly machinery and its substrate Fe-S proteins is frequently associated with human diseases.[21]

Crosstalk between Fe-S cluster biogenesis and iron homeostasis has been extensively documented in numerous organisms. Studies in *S. cerevisiae* have revealed that the iron-responsive transcription factor Aft1, involved in the activation of iron regulon, interacts with yeast [2Fe-2S] binding glutaredoxin Grx3. Of importance, deletion of *GRX3* and *GRX4* leads to intracellular iron overload resulting from constitutive activation of the iron regulon.[22] In mammalian cells, cellular iron homeostasis is maintained by iron-regulatory proteins IRP1 and IRP2 that bind iron-response elements (IREs) in key target mRNAs during iron depleted conditions, leading to increased iron uptake and the release of stored iron. The CIA pathway regulates cellular iron homeostasis by both modulating the FBXL5-dependent degradation of IRP2 and facilitating Fe-S cluster incorporation into IRP1 which inhibits its IRE-binding activity.[20,23,11] Furthermore, NUBP1 depletion has been shown to compromise maturation of extra-mitochondrial Fe-S proteins leading to perturbation in cellular levels of ferritin, transferrin receptor and uptake of transferrin[11].

The emerging understanding of Fe-S cluster biogenesis benefits from the availability of a diverse set of techniques. The binding of Fe-S clusters in proteins is usually determined by the incorporation of radioactive ^{55}Fe or measured by spectroscopic approaches such as UV-Vis and electron paramagnetic resonance.[24,25] Native mass spectrometry, with its ability to preserve noncovalent interactions, has also been exploited to detect Fe-S cluster binding of proteins.[26] With these tools to evaluate cluster binding, Fe-S proteins as well as machineries required for Fe-S cluster biogenesis have been identified and characterized. The application of affinity purification coupled with bottom-up proteomics is also very commonly used to discover additional components of the machineries that are essential for Fe-S cluster biogenesis.[5,15,20]

Bottom-up Proteomics

Bottom-up proteomics is the proteome-wide characterization of proteins by mass spectrometry based on analysis of analytes at the peptide-level.[27] With advances in both hardware and software, bottom-up proteomics now contains a comprehensive set of tools to investigate questions in biological sciences. The applications of bottom-up proteomics include but is not limited to assessing post-translational modifications, probing protein-protein interactions, and analyzing protein structures. The general workflow of bottom-up proteomics typically begins with the solubilization of proteins from biological materials followed by the tryptic digestion of the protein mixture. The digested tryptic peptides are then separated by reversed phase chromatography, ionized using electrospray ionization, and detected by a mass spectrometer.

Approaches that are generally used for peptide analysis on a mass spectrometer are data-dependent acquisition (DDA), data-independent acquisition (DIA) and targeted

acquisition.[28] In DDA, a full MS scan (MS1) is first acquired to detect the mass-to-charge ratio (m/z) of intact peptides at a given point in the chromatographic separation. The detected peptide precursors are ranked by intensity, sequentially selected by quadrupole isolation, and fragmented. The acquired fragmentation spectra (MS2) are interpreted by database search algorithms to provide sequence information of the peptide analytes. This acquisition scheme, although enabling the detection of massive number of analytes, is stoichiometrically biased. In contrast, targeted acquisition of monitors a panel of peptide precursors preselected by the user from proteins of interest. Selected precursors are isolated by quadrupole and fragmented. This acquisition scheme enables increased sensitivity for the selected analytes especially when they are at low abundance.

Bottom-up mass spectrometry is widely used not only for detection but also quantification of analytes. Peptide and protein quantification by bottom-up proteomics can be achieved either by labeled or label-free approaches. The label-free approach can be further divided into two categories: by spectral count or by intensity. Spectral count, as is indicated by its name, is simply the number of spectra identified for a certain protein. Spectral count-based quantification is considered rough estimation of protein abundance due to many reasons, including the skewed linearity from dynamic exclusion.[29] Intensity-based quantification utilizes the area under the chromatographic elution peak for peptides of interest to evaluate the abundance of the analyte across samples. The peaks for quantification are determined either by directly detecting LC-MS features or generating extracted ion chromatography from identification information.[30,31] The intensity-based quantification is further extended to intensity based absolute

quantification (iBAQ) of proteins by summing all peptide peak intensities and divide it by the number of theoretically observable tryptic peptides.[32]

Reference

1. Johnson, M. K. & Smith, A. D. Iron-Sulfur Proteins. in *Encyclopedia of Inorganic and Bioinorganic Chemistry* (John Wiley & Sons, Ltd, 2011). doi:10.1002/9781119951438.eibc0109.
2. Beinert, H., Holm, R. H. & Munck, E. Iron-Sulfur Clusters: Nature's Modular, Multipurpose Structures. *Science (80-.).* **277**, 653–659 (1997).
3. Read, A. D., Bentley, R. E., Archer, S. L. & Dunham-Snary, K. J. Mitochondrial iron–sulfur clusters: Structure, function, and an emerging role in vascular biology: Mitochondrial Fe-S Clusters – a review. *Redox Biology* vol. 47 (2021).
4. Syed, A. & Tainer, J. A. Charge Transport Communication through DNA by Protein Fe-S Clusters: How Far Is Not Too Far? *ACS Cent. Sci.* **5**, 7–9 (2019).
5. Stehling, O. *et al.* MMS19 Assembles Iron-Sulfur Proteins Required for DNA Metabolism and Genomic Integrity. *Science (80-.).* **337**, 195–199 (2012).
6. Fuss, J. O., Tsai, C. L., Ishida, J. P. & Tainer, J. A. Emerging critical roles of Fe-S clusters in DNA replication and repair. *Biochim. Biophys. Acta - Mol. Cell Res.* **1853**, 1253–1271 (2015).
7. Eisenstein, R. S. *IRON REGULATORY PROTEINS AND THE MOLECULAR CONTROL OF MAMMALIAN IRON METABOLISM*. www.annualreviews.org (2000).
8. Beinert, H., Kennedy, M. C. & Stout, D. *Aconitase as Iron−Sulfur Protein, Enzyme, and Iron-Regulatory Protein*. https://pubs.acs.org/sharingguidelines.
9. Kiley, P. J. & Beinert, H. The role of Fe-S proteins in sensing and regulation in bacteria. *Current Opinion in Microbiology* vol. 6 181–185 (2003).

10. Andreini, C., Putignano, V., Rosato, A. & Banci, L. The human iron-proteome. *Metallomics* **10**, 1223–1231 (2018).

11. Pérard, J. & Ollagnier de Choudens, S. Iron–sulfur clusters biogenesis by the SUF machinery: close to the molecular mechanism understanding. *Journal of Biological Inorganic Chemistry* vol. 23 581–596 (2018).

12. Lill, R. *et al.* The role of mitochondria and the CIA machinery in the maturation of cytosolic and nuclear iron-sulfur proteins. *Eur. J. Cell Biol.* **94**, 280–291 (2015).

13. Braymer, J. J. & Lill, R. Iron–sulfur cluster biogenesis and trafficking in mitochondria. *J. Biol. Chem.* **292**, 12754–12763 (2017).

14. Maio, N. & Rouault, T. A. Outlining the Complex Pathway of Mammalian Fe-S Cluster Biogenesis. *Trends Biochem. Sci.* **45**, 411–426 (2020).

15. Patel, S. J. *et al.* A PCBP1–BolA2 chaperone complex delivers iron for cytosolic [2Fe–2S] cluster assembly. *Nat. Chem. Biol.* **15**, 872–881 (2019).

16. Frey, A. G., Palenchar, D. J., Wildemann, J. D. & Philpott, C. C. A glutaredoxin-BolA complex serves as an iron-sulfur cluster chaperone for the cytosolic cluster assembly machinery. *J. Biol. Chem.* **291**, 22344–22356 (2016).

17. Netz, D. J. A., Pierik, A. J., Stümpfig, M., Mühlenhoff, U. & Lill, R. The Cfd1-Nbp35 complex acts as a scaffold for iron-sulfur protein assembly in the yeast cytosol. *Nat. Chem. Biol.* **3**, 278–286 (2007).

18. Balk, J., Pierik, A. J., Aguilar Netz, D. J., Mühlenhoff, U. & Lill, R. The hydrogenase-like Nar1p is essential for maturation of cytosolic and nuclear iron-sulphur proteins. *EMBO J.* **23**, 2105–2115 (2004).

19. Gari, K. *et al.* MMS19 Links Cytoplasmic Iron-Sulfur Cluster Assembly to DNA

Metabolism. **3801**, 2011–2013 (2012).

20. Stehling, O. *et al.* Human CIA2A-FAM96A and CIA2B-FAM96B integrate iron homeostasis and maturation of different subsets of cytosolic-nuclear iron-sulfur proteins. *Cell Metab.* **18**, 187–198 (2013).
21. Sheftel, A., Stehling, O. & Lill, R. Iron-sulfur proteins in health and disease. *Trends Endocrinol. Metab.* **21**, 302–314 (2010).
22. Outten, C. E. & Albetel, A. N. Iron sensing and regulation in Saccharomyces cerevisiae: Ironing out the mechanistic details. *Curr. Opin. Microbiol.* **16**, 662–668 (2013).
23. Mayank, A. K. *et al.* An Oxygen-Dependent Interaction between FBXL5 and the CIA-Targeting Complex Regulates Iron Homeostasis. *Mol. Cell* **75**, 382-393.e5 (2019).
24. Freibert, S. A. *et al.* Biochemical Reconstitution and Spectroscopic Analysis of Iron–Sulfur Proteins. in *Methods in Enzymology* vol. 599 197–226 (Academic Press Inc., 2018).
25. Lill, R., Srinivasan, V. & Mühlenhoff, U. The role of mitochondria in cytosolic-nuclear iron-sulfur protein biogenesis and in cellular iron regulation. *Curr. Opin. Microbiol.* **22**, 111–119 (2014).
26. Fontecilla-Camps, J. C. & Nicolet, Y. *Metallo-proteins Methods and Protocols Methods in Molecular Biology 1122*. http://www.springer.com/series/7651.
27. Zhang, Y., Fonslow, B. R., Shan, B., Baek, M. C. & Yates, J. R. Protein analysis by shotgun/bottom-up proteomics. *Chemical Reviews* vol. 113 2343–2394 (2013).
28. Gillet, L. C., Leitner, A. & Aebersold, R. Mass Spectrometry Applied to Bottom-Up

Proteomics: Entering the High-Throughput Era for Hypothesis Testing. *Annual Review of Analytical Chemistry* vol. 9 449–472 (2016).

29. Lundgren, D. H., Hwang, S. Il, Wu, L. & Han, D. K. Role of spectral counting in quantitative proteomics. *Expert Review of Proteomics* vol. 7 39–53 (2010).
30. Tyanova, S., Temu, T. & Cox, J. The MaxQuant computational platform for mass spectrometry-based shotgun proteomics. *Nat. Protoc.* **11**, 2301–2319 (2016).
31. MacLean, B. *et al.* Skyline: An open source document editor for creating and analyzing targeted proteomics experiments. *Bioinformatics* **26**, 966–968 (2010).
32. Schwanhüusser, B. *et al.* Global quantification of mammalian gene expression control. *Nature* **473**, 337–342 (2011).

Figure 1. Overview of the Cytosolic Iron-Sulfur Cluster Assembly (CIA) Pathway

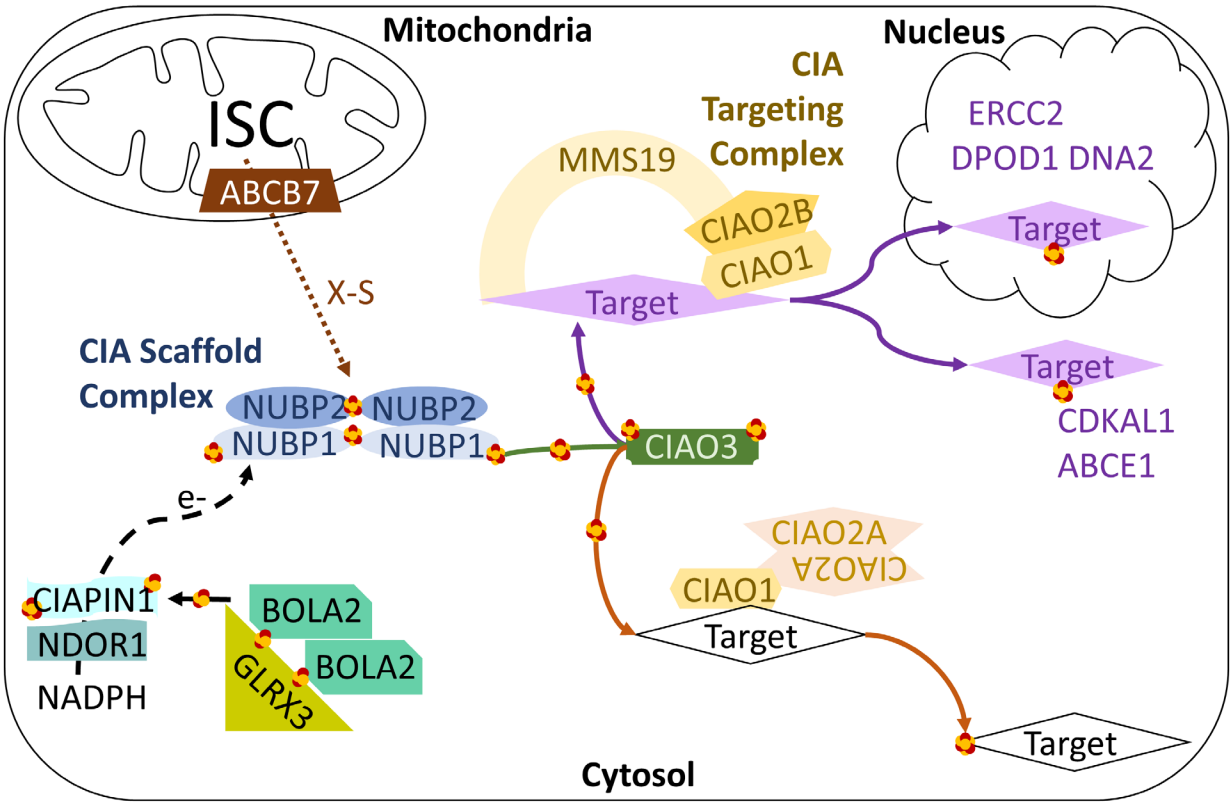

CHAPTER 2

Iron-Regulated Assembly of the Cytosolic Iron-Sulfur Cluster Biogenesis Machinery

This chapter is adapted from the following manuscript with minor changes.

Fan X, Barshop WD, Vashisht AA, Pandey V, Leal S, Rayatpisheh S, Jami-Alahmadi Y, Sha J, Wohlschlegel JA (2022). Iron-Regulated Assembly of the Cytosolic Iron-Sulfur Cluster Biogenesis Machinery. *J Biol Chem*. DOI: 10.1016/j.jbc.2022.102094.

Iron-Regulated Assembly of the Cytosolic Iron-Sulfur Cluster Biogenesis Machinery

Xiaorui Fan (范 潇蕊)[1,2], William D. Barshop[1#], Ajay A. Vashisht[1$], Vijaya Pandey[1], Stephanie Leal[1&], Shima Rayatpisheh[1$], Yasaman Jami-Alahmadi[1], Jihui Sha[1], James A. Wohlschlegel[1*]

[1]Department of Biological Chemistry, David Geffen School of Medicine and [2]Molecular Biology Institute, University of California, Los Angeles, CA 90095, USA

Present address: [#]Thermo Fisher Scientific, San Jose, CA; [$]Genomics Institute of The Novartis Research Foundation, San Diego, CA; [&]University of California - San Diego, San Diego, CA

[*] Address correspondence to James A. Wohlschlegel. E-mail: jwohl@mednet.ucla.edu

Running title

Assembly of CIA Complexes Regulated by Iron

Keywords

Iron-sulfur protein, metalloprotein, protein-protein interaction, proteomics, redox regulation, cytosolic iron-sulfur cluster assembly (CIA)

Abstract

The cytosolic iron-sulfur (Fe-S) cluster assembly (CIA) pathway delivers Fe-S clusters to nuclear and cytosolic Fe-S proteins involved in essential cellular functions. Although the delivery process is regulated by the availability of iron and oxygen, it remains unclear how CIA components orchestrate the cluster transfer under varying cellular environments. Here, we utilized a targeted proteomics assay for monitoring CIA factors and substrates to characterize the CIA machinery. We find that NUBP1 (NBP35),

CIAO3 (NARFL) and CIA substrates associate with NUBP2 (CFD1), a component of the CIA scaffold complex. We also show that NUBP2 weakly associates with the CIA targeting complex (MMS19, CIAO1, CIAO2B) indicating the possible existence of a higher order complex. Interactions between CIAO3 and the CIA scaffold complex are strengthened upon iron supplementation or low oxygen tension, while iron chelation and reactive oxygen species weaken CIAO3 interactions with CIA components. We further demonstrate that CIAO3 mutants defective in Fe-S cluster binding fail to integrate into the higher order complexes. However, these mutants exhibit stronger associations with CIA substrates under conditions in which the association with the CIA targeting complex is reduced suggesting that CIAO3 and CIA substrates may associate in complexes independently of the CIA targeting complex. Together, our data suggest that CIA components potentially form a metabolon whose assembly is regulated by environmental cues and requires Fe-S cluster incorporation in CIAO3. These findings provide additional evidence that the CIA pathway adapts to changes in cellular environment through complex reorganization.

Introduction

Iron-sulfur (Fe-S) clusters are ubiquitous cofactors utilized by all realms of life, among which [2Fe-2S] and [4Fe-4S] clusters are the most commonly found in biological systems.[1] These cofactors play a role in maintaining protein stability, as well as regulating subcellular localization and enzymatic activity.[2–4] Being redox sensitive, these clusters also serve as redox centers to facilitate electron transfer. The redox states of Fe-S clusters change in response to environmental stimuli, which provides an additional layer of regulation of protein function.[1,4] In eukaryotic organisms, the biogenesis of Fe-S

clusters is highly compartmentalized with distinct branches of the biogenesis pathway responsible for the maturation of mitochondrial and extramitochondrial Fe-S proteins.[5,6] The maturation of extramitochondrial Fe-S proteins is facilitated specifically by the cytosolic Fe-S cluster biogenesis pathway (CIA). The CIA pathway is associated with a plethora of cellular processes including cell proliferation, DNA damage repair, non-sense mediated decay, apoptosis and microtubule-based processes such as ciliogenesis.[2,7–11] Deregulation of CIA components and substrates has also been linked to numerous human diseases.[5,12,13]

The maturation of cytosolic Fe-S proteins is a multi-step process that is tightly regulated. In human cells, bioavailable iron is delivered for [2Fe-2S] cluster biogenesis by poly(rC)-binding protein 1 (PCBP1) to the chaperone consisting of the BolA-like protein 2 (BOLA2) and glutaredoxin-3 (GLRX3).[14] [4Fe-4S] clusters are first assembled on the CIA scaffold complex composed of NUBP1 and NUBP2.[11,15] This step requires an unknown sulfur containing compound that is produced by the mitochondrial Fe-S cluster biogenesis (ISC) machinery and transported to the cytosol through the mitochondrial inner membrane protein ABCB7. This transiently bound [4Fe-4S] cluster is then transferred to the cluster carrier protein CIAO3 and eventually incorporated into apoprotein substrates through the activity of the CIA targeting complex composed of MMS19, CIAO1 and CIAO2B.[2,16]

Although the crosstalk has been extensively documented in numerous organisms between Fe-S cluster biogenesis and the cellular environment such as intracellular iron and oxygen levels, evidence supporting this idea is only just beginning to emerge in humans.[1,4] The availability of bioavailable iron was recently shown to regulate cytosolic

[2Fe-2S] cluster biogenesis by controlling the association of BOLA2 and GLRX3.[17] Additionally, the maturation of specific extramitochondrial Fe-S proteins involved in DNA repair and iron homeostasis are regulated by iron and oxygen availability.[18,19] Despite these advances, however, the mechanisms underlying much of this regulation are still unknown.

In this work, we developed a targeted proteomics assay that monitor proteins in the CIA pathway. Using this assay, we were able to detect the association of the CIA targeting complex (MMS19, CIAO1 and CIAO2B) and CIA substrates (DNA2, POLD1, CDKAL1 and ERCC2) with the CIA scaffold complex component NUBP2. We also find that the interaction of CIAO3 with the CIA scaffold complex is regulated by acute changes in cellular environment, including changes in the labile iron pool, exposure to reactive oxygen species (ROS) and changes in oxygen tension. The interaction of CIAO3 with the CIA targeting complex, although minimally affected by these acute environmental changes, is dependent on Fe-S cluster binding by CIAO3. CIAO3 mutants that are defective in Fe-S cluster binding display impaired association with the rest of the CIA machinery. Together, these data suggest the formation of CIA metabolon composed of the CIA scaffold complex, CIAO3, the CIA targeting complex and CIA substrates. The metabolon assembly is dynamic and regulated by environmental cues, possibly through altering Fe-S clusters in CIAO3.

Results

Formation of the CIA Metabolon – In order to investigate how the CIA pathway responds to changes in cellular environment, we began by comparing the endogenous protein levels of major CIA components in cells exposed to iron supplementation or

chelation, mimicking an iron sufficient or deficient environment. Cells were treated with ferric ammonium citrate (FAC) or the iron chelator deferoxamine mesylate (DFO) for 8 hours and whole cell lysates were probed with antibodies against CIA components as well as two known substrates. Protein levels for F-box/LRR-repeat protein 5 (FBXL5), an E3 ligase that accumulates when sufficient iron is present, and iron-responsive element-binding protein 2 (IREB2/IRP2), an FBXL5 substrate that is stabilized by iron depletion, served as treatment controls for FAC and DFO, respectively.[20] We did not observe significant changes in the steady state levels of either CIA components or CIA substrates in this time frame (Fig. 2-1A). Although defects in Fe-S cluster incorporation have been previously shown to cause destabilization of a number of Fe-S proteins, these effects are typically observed either as a result of chronic ablation of the Fe-S cluster assembly machinery or in mutant proteins defective in cluster incorporation.[2,21]

Since we did not observe any immediate effect of changes in intracellular iron levels on the stability of CIA factors and substrates, we next examined interactions between CIA components under basal conditions. Multiple independent studies have shown that components of the CIA targeting complex are detected in higher order complexes ranging in molecular weight from 400 to 1000kDa.[16,22,23] Components of the CIA targeting complex interact with CIAO3, which in turn interacts with the CIA scaffold complex, indicating that these CIA components may be organized into higher order complexes. To examine this possibility, we performed affinity purification of NUBP2, a component of the CIA scaffold complex, and characterized proteins associated with NUBP2 using an unbiased shotgun proteomic approach. In addition to NUBP1 and CIAO3 which are known NUBP2 interactors, we also detected two components of the

CIA targeting complex (CIAO1 and MMS19) as well as CIA substrates (CDKAL1 and ELP3) in the NUBP2 immunoprecipitates (Fig. 2-1B). CIAO2B, another component of the targeting complex, was not identified in this analysis, although this could be due to poor sampling of low abundance peptides. To address this potential issue, we developed a targeted proteomics assay (tier 3) that utilizes parallel reaction monitoring to assess the presence and abundance of a panel of proteins relevant to the Fe-S cluster assembly pathways.[24] We first tested this assay on a serially diluted peptide standard prepared from HEK293 whole cell extracts and were able to detect the presence and estimate the relative abundance of known CIA factors (ABCB7, BOLA2, GLRX3, CIAPIN1, NUBP1, NUBP2, CIAO3, MMS19, CIAO1, CIAO2B and CIAO2A) and several prototypical CIA substrates (ABCE1, CDKAL1, ERCC2 and POLD1) (Fig. 2-1C). This targeted approach, which provides better sensitivity and quantitation than unbiased proteomics assays, was then applied to NUBP2 immunoprecipitates to specifically monitor diagnostic peptides derived from components of the CIA scaffold complex (NUBP1 and NUBP2), CIAO3, components of the CIA targeting complex (MMS19, CIAO1 and CIAO2B) and CIA substrates (CDKAL1, DNA2, ERCC2, ABCE1 and POLD1). Diagnostic peptides utilized in this analysis are listed in Table 2-1. As expected, NUBP1 and CIAO3 were identified as interacting proteins (Fig. 2-1D and Table 2-2). All components of the CIA targeting complex (MMS19, CIAO1 and CIAO2B) were also found associated with NUBP2. In addition, we observed that CIA substrates CDKAL1, DNA2, ERCC2 and POLD1 copurified with NUBP2 (Fig. 2-1D). These observations together suggest that the CIA scaffold complex, CIAO3, the CIA targeting complex and CIA substrates potentially assemble into a higher order protein assembly

that facilitates Fe-S cluster transfer into substrates. The assembly is likely dynamic, given that formaldehyde crosslinking enhanced the association between the CIA scaffold complex and the CIA targeting complex (Fig. 2-1E).

Iron Regulation of CIAO3 Interactome – To determine the influence of intracellular iron availability on the assembly of CIA complexes, we utilized affinity purification of CIAO3 followed by tandem mass spectrometry to compare the CIAO3 interactome between iron replete and iron depleted conditions. These proteomics studies were done using both standard unbiased protein identification followed by label-free quantitation as well as our targeted proteomics assay that specifically measures the abundance of a panel of key Fe-S machinery proteins and substrates. The unbiased proteomics analysis demonstrated that interactions between CIAO3 and multiple proteins depend on the availability of labile iron, including both components of the CIA scaffold complex (NUBP1 and NUBP2) (Fig. 2-2A and Table 2-3). In contrast, interactions between CIAO3 and the CIA targeting complex were minimally affected by cellular iron levels (Fig. 2-2A). These results were validated by our targeted proteomics assay in which parallel reaction monitoring was used to detect and quantify the levels of the CIA scaffold complex and the CIA targeting complex present in CIAO3 immunoprecipitates isolated from iron replete and iron depleted conditions. We confirmed that CIAO3 interacts with NUBP1 and NUBP2 in an iron-dependent manner and observed that both CIAO3-NUBP1 and CIAO3-NUBP2 interactions were reduced ~4-fold in iron-deficient conditions indicating that CIAO3 dissociates from the intact CIA scaffold complex (Fig. 2-2B). Conversely, interactions between CIAO3 and the CIA targeting complex were only subtly influenced by iron levels and did not reach statistical significance (Fig. 2-3C).

To validate that endogenous CIAO3 also interacts with the CIA scaffold complex in an iron-dependent manner, we treated cells expressing 3HA-3FLAG tagged NUBP2 with ferric ammonium citrate or deferoxamine mesylate, immunoprecipitated NUBP2 from whole cell lysate using anti-HA beads and immunoblotted with CIAO3 antibodies. Our data show that the CIAO3-NUBP2 interaction is stabilized by the addition of iron and impaired when iron is depleted through chelation (Fig. 2-2D).

We further characterized the association between CIAO3 and its interactors in response to alterations in intracellular iron levels after different time periods of treatment. We treated cells expressing 3HA-3FLAG-CIAO3 with FAC or DFO for either 3 or 8 hours. We performed anti-HA immunoprecipitation followed by immunoblotting with indicated antibodies (Fig. 2-2E). Our data showed that the CIAO3-NUBP2 interaction increased after 3 hours of FAC treatment but slightly declined by 8 hours of treatment. Iron chelation caused a strong reduction in NUBP2 binding to CIAO3 as early as 3 hours after treatment with DFO and extended up to at least 8 hours after treatment. Ferritin levels, as expected, were gradually increasing over the same time period. These observations suggest that the response of the CIAO3-NUBP2 interaction to changes in iron levels is rapid.

CIAO3 Interactions are Redox-regulated – Given the observation that CIAO3's interactome was regulated by iron availability, we next examined whether these interactions were also influenced by other environmental stimuli. First, we treated cultured cells with reactive oxygen species and examined the effects on the CIAO3 interactome. Tert-butyl hydroperoxide (tBHP) oxidizes glutathione and induces oxidative stress.[25] After cells were exposed to tBHP for 4 hours, 3HA-3FLAG tagged CIAO3 was

immunoprecipitated from whole cell extracts and immunoblotted with antibodies against both the CIA scaffold complex and the CIA targeting complex. We observed a diminished CIAO3 interaction with the CIA scaffold complex under oxidative stress (Fig. 2-3A). A decreased interaction between CIAO3 and the CIA targeting complex was also observed but was comparatively modest under the same conditions. In addition to oxidative stress, we also manipulated oxygen tension and examined its effect on CIAO3 interactions. We immunoprecipitated 3HA-3FLAG-CIAO3 from extracts derived from cells cultured in either 21% O_2 or 1% O_2 and determined its interactions by immunoblotting with antibodies of NUBP2. HIF1α served as a positive control for hypoxia. We found that the CIAO3-NUBP2 interaction was stabilized in cells cultured in 1% O_2 (Fig. 2-3B). Together these results suggest that CIAO3 containing complexes are sensitive to the redox status of the cell.

The versatile nature of Fe-S clusters allows them to sense changes in both intracellular iron availability and the redox status of the cell.[1,26] As such, we hypothesized that the ability of these environmental changes to influence CIAO3 interactions might stem from effects on the Fe-S clusters bound to CIAO3 or other key components of this pathway. To test this possibility, we examined how disruption of Fe-S cluster biogenesis pathways affected the CIAO3 interactome. Previous studies have shown that cytosolic Fe-S cluster biogenesis mediated by the CIA pathway depends on mitochondrial Fe-S cluster biogenesis by the ISC pathway and that depleting the ISC scaffold protein, ISCU, leads to reduced iron incorporation and protein stability of both CIAO3 and CIA substrates.[2,27] We depleted ISCU1/2 from cells using RNAi and then induced expression of 3HA-3FLAG-CIAO3 which was stably expressed under the

control of a doxycycline-inducible promoter. We observed a reduced amount of CIAO3 in the cells with silenced ISCU1/2, which is consistent with previous observations (Fig. 2-3C).[2] Immunoblots of the affinity purified CIAO3 complexes showed reduced co-precipitation for both the CIA scaffold complex and the CIA targeting complex. Densitometric evaluation of CIAO3 interactions as shown in Fig. 2-3C revealed >60% and >90% reduction in the amount of NUBP1 and NUBP2 co-purifying with CIAO3 in response to the silencing of ISCU1/2 (Fig. 2-3D). In addition, we observed that the interactions between CIAO3 and components of the CIA targeting complex also drastically diminished upon knockdown of ISCU1/2 (Fig. 2-3E). Together, our observations demonstrate the assembly of CIAO3 into higher order complexes depends on the presence of a functional Fe-S cluster biogenesis pathway.

Fe-S Cluster Incorporation of CIAO3 Regulates its Interactions -- CIAO3, which plays an essential role in bridging early and late CIA steps, has two Fe-S cluster binding sites: one at its N-terminus and the other at its C-terminus.[28,29] Given that Fe-S clusters are intrinsically sensitive to the cellular environment and regulate the stability and/or function of Fe-S proteins, we reasoned that CIAO3 interactions may be regulated by its cluster incorporation status. Previous studies have indicated that missense mutations of CIAO3 substituting cysteine with serine at position 71 in the N-terminus, or at both positions 190 and 395 in the C-terminus render the protein defective in binding of Fe-S clusters.[28,29] Based on these studies, we generated CIAO3 mutants with impaired cluster incorporation (C71S, C190S/C395S and C71S/C190S/C395S) to determine whether the Fe-S cluster requirement observed for CIAO3 interactions was dependent on cluster binding by CIAO3 itself (Fig. 2-4A). To compare and quantify the

interactomes of wildtype and mutant versions of CIAO3 with known CIA components, we utilized our PRM-based targeted proteomics assay that monitors known CIA components and substrates as described earlier. We purified both wildtype and mutant 3HA-3FLAG CIAO3 complexes and quantified their interactions with the CIA scaffold complex, the CIA targeting complex and CIA substrates after normalization to the amount of CIAO3 present in each purification. We observed that CIAO3-NUBP1/2 interactions were dramatically reduced for more than 32-fold, consistent with our earlier observation that Fe-S clusters are required for the interaction between CIAO3 and the CIA scaffold complex (Fig. 2-4B). The CIA targeting complex also showed modestly reduced association with CIAO3 displaying an approximately 5-fold decrease for the C71S mutant, a 3 to 4-fold decrease for the C190S/C395S mutant, and a 2-fold change in the C71S/C190S/C395S mutant (Fig. 2-4C). Intriguingly, we observed that the association of substrates like ABCE1 and CDKAL1 with CIAO3 strongly increased when the CIAO3 C-terminal Fe-S cluster binding site was mutated (Fig. 2-4D), which suggests that CIAO3 may also associate with CIA substrates independently of the CIA targeting complex. Of note, we previously generated a mutant of ERCC2 lacking amino acids 277 to 286 that cannot bind to the CIA targeting complex.[18] We show here that this ERCC2 mutant associated more weakly with CIAO3 relative to wild-type ERCC2, suggesting that CIAO3 binding by ERCC2 requires the CIA targeting complex binding region of ERCC2 and is consistent with the model that the CIA scaffold complex, CIAO3, the CIA targeting complex and CIA substrates form higher order complexes that facilitates Fe-S protein maturation (Fig. 2-4E). These results together provide evidence that Fe-S

cluster incorporation into CIAO3 controls its interactions and governs its incorporation in CIA metabolon.

Disease Associated CIAO3 Mutant Fails to Assemble into CIA Metabolon – A mutation in CIAO3 (S161I) has recently been reported to associate with diffuse pulmonary arteriovenous malformations (PAVMs).[30] Homology modeling of human CIAO3 based on Fe-only hydrogenase of *Clostridium pasteurianum* (1FEH) revealed that this evolutionally conserved serine 161 is ~3.1Å from an evolutionally conserved proline (P215) and 11.3Å from the C-terminus Fe-S cluster (Fig. 2-5A and 2-5B).[31] Therefore, we hypothesized that the CIAO3-S161I mutation might perturb Fe-S cluster binding due to either the loss of serine-proline hydrogen bonding or sterically hindering cluster binding in the C-terminus site. In this case, the CIAO3-S161I would behave phenotypically like the C-terminal site CIAO3 mutants (C190S/C395S and C71S/C190S/C395S) with decreased binding to the CIA scaffold complex and the CIA targeting complex but increased binding to CIA substrates. To test this, we immunoprecipitated both wild-type and S161I versions of 3HA-3FLAG-CIAO3 and probed the immunoprecipitates for components of the CIA scaffold complex (NUBP1 and NUBP2), components of the CIA targeting complex (MMS19, CIAO1 and CIAO2B) and CIA substrates (CDKAL1 and ERCC2) (Fig. 2-5C). Relative to wild-type CIAO3, the interactions of CIAO3-S161I with both the CIA scaffold complex and the CIA targeting complex were significantly reduced (Fig. 2-5D and Fig. 2-5E), while its association with CIA substrates increased (Fig. 2-5F), reminiscent of C190S/C395S and C71S/C190S/C395S mutants. These findings suggest that the failure of CIAO3-S161I to

incorporate into a higher order complex may contribute to the disease phenotype associated with PAVMs.

Discussion

The CIA pathway facilitates Fe-S cluster incorporation into a plethora of extramitochondrial Fe-S proteins involved in a variety of essential cellular functions. It remains a key question how the CIA pathway adapts to different cellular environments to achieve precise control of substrate maturation. In this study, we describe a novel axis of regulation for cytosolic [4Fe-4S] cluster biogenesis (Fig. 2-6). Utilizing a targeted proteomics assay to assess known components and substrates of the CIA pathway, we demonstrate the existence of higher order CIA complexes containing the CIA scaffold complex, CIAO3, the CIA targeting complex and CIA substrates. These higher order complexes are sensitive to acute environmental changes and are reorganized in response to changes in the labile iron pool, oxygen tension, and ROS. Our data further show that Fe-S cluster binding by CIAO3 is required for its interactions with the CIA scaffold complex and the CIA targeting complex. Finally, we demonstrate that the CIAO3-S161I mutant associated with diffuse pulmonary arteriovenous malformation fails to incorporate into a functional CIA complex highlighting the physiological and pathological relevance of this pathway.

Although an understanding of the components and the organization of the CIA pathway has begun to emerge, still very little is known about the dynamics of the pathway and how it responds to different cellular and environmental cues, especially in the mammalian system. A previous study has demonstrated that the association of BOLA2 with GLRX3 in the context of the cytosolic [2Fe-2S] cluster biogenesis

machinery is iron-dependent and highlights one important mode of regulation.[17] Our study further extends this paradigm by showing that the association of CIAO3 with the CIA scaffold complex is tightly coupled to cellular iron levels with iron strongly promoting the assembly. The regulated binding of CIAO3 with the CIA scaffold complex is also influenced by ROS and hypoxia suggesting that it is broadly responsive to changes in cellular conditions. These data suggest that the CIA pathway adapts to acute environmental cues through the reorganization of a higher order CIA complex via a mechanism by which the CIA scaffold complex dynamically joins/leaves the rest of the complex.

Unlike acute environmental changes that primarily alter CIAO3's association with the CIA scaffold complex, compromised Fe-S cluster biogenesis and improper cluster incorporation in CIAO3 prohibited both the CIA scaffold complex and the CIA targeting complex from interacting with CIAO3. We therefore reasoned that the two Fe-S clusters in CIAO3, directly or indirectly, sense the changes in the cellular environment and subsequently regulate the dynamic assembly of the CIA machinery. Homology structural modeling predicts that the N-terminus Fe-S cluster of CIAO3 is solvent exposed while the C-terminus cluster is buried in the center of the protein. We speculate that these clusters play different roles in regulating CIAO3 behavior with the solvent exposed N-terminal Fe-S cluster responding to acute changes in the cellular environment to modulate CIAO3 interactions, and the C-terminal cluster being required for the structural integrity of the protein but having limited capacity for immediate environmental sensing due to its solvent inaccessibility. The CIAO3-S161I mutant was found to associate with diffuse PAVMs.[30] Based on our predicted structure of CIAO3,

substituting Ser with Ile at residue 161 would disrupt the C-terminal integrity of protein and likely phenocopy mutants with defective C-terminal Fe-S cluster incorporation. As expected, we observed a reduction in protein levels for the CIAO3-S161I mutant. This mutant also interacts weakly with the CIA scaffold complex and the CIA targeting complex. These findings are consistent with the model that the C-terminus cluster of CIAO3 mediates its stability and that Fe-S cluster binding in CIAO3 is required for its incorporation into CIA machineries. The CIAO3-S161I mutation in patients likely disrupts cytosolic Fe-S cluster biogenesis and potentially contributes to the molecular basis of PAVMs.

Experimental procedures

Plasmids and Primers

Plasmid containing wild type human CIAO3 was purchased from Open Biosystems (Clone: 5242707). cDNA was amplified using Phusion polymerase with the primer pair containing attB recombination sites (5'-GGGGACAAGTTTGTACAAAAAAGCAGGCTTCATGGCGTCGCCCTTCAGC-3'; 5'-GGGGACCACTTTGTACAAGAAAGCTGGGTCCTACCACCGGATGCCCAG-3'). Using the Gateway Recombination Cloning Technology, CIAO3 was cloned into pDONR221 vector and subsequently into the destination vector pcDNA5/FRT encoding a N-terminus tandem 3xHA-3xFLAG tag. CIAO3-C71S, CIAO3-C190S/C395S, CIAO3-C71S/C190S/C395S, CIAO3-S161I were generated using Quikchange Mutagenesis (Agilent) with primer pairs containing the mutated nucleotides (C71S: 5'-CTAAACGACTCCCTGGCGTGC-3', 5'-GCACGCCAGGGAGTCGTTTAG-3'; C190S: 5'-GCCTCTGCCTCCCCAGGCTGG-3', 5'-CCAGCCTGGGGAGGCAGAGGC-3'; C395S:

5’-GTCATGGCCTCCCCCTCAGGC-3’, 5’- GCCTGAGGGGGAGGCCATGAC-3’; S161I: 5'-CTCTCCAGGAGGATGAAGTGCCTTGAGAAGGC-3', 5'-GCCTTCTCAAGGCACTTCATCCTCCTGGAGAG-3'). Mutations were verified by sequencing with M13F and M13R primers.

Cell Culture, Cell Lines, Transfection, and Treatments

HEK293 cells were obtained from the American Type Culture Collection. The Flp-In™ T-REx™ 293 cell line obtained from ThermoFisher Scientific was used to generate HEK293 cells stably expressing 3xHA-3xFLAG tagged wild type and mutant CIAO3 using the Flp-In™ System. Cells were cultured in Dulbecco’s Modified Eagle’s Medium (Gibco™ 11960-044) supplemented with 10% fetal bovine serum (Gemini Bio-products Foundation B™ 900-208), 2mM L-Glutamine (Gibco™ 25030-081), with or without 1X Antibiotic-Antimycotic (Gibco™ 15240-062) at 37°C. Cells grown under normoxic conditions were cultured in ambient air with 5% CO_2. Hypoxic conditions were maintained by culturing cells for 16 hours in a hypoxia chamber (STEMCELL technologies) equilibrated with a gas mixture containing 1% O_2, 5% CO_2 and 94% N_2 at a flow rate of 20L/min for 7 minutes using the Single Flow Meter (STEMCELL Techonologies, Cat #27311) and then sealed till harvesting. The Flp-In™ T-REx™ 293 cell lines were treated with 1µg/ml doxycycline (Fisher Bioreagents #BP26535) for about 24 hours to induce protein expression. Cells were treated with drugs including 100µg/ml ferric ammonium citrate (FAC, Fisher Bioreagents CAS 1185-57-5), 100µM deferoxamine mesylate salt (DFO, Sigma D9533-1G) or 100µM tert-Butyl hydroperoxide (tBHP, Aldrich 458139-100ML, Lot # MKCD3313). Knockdown of ISCU1/2 was achieved by transfecting cells with siGENOME Human ISCU siRNA (Dharmacon™

15240-062 SMARTPool M-012837-03-0005) using the Lipofectamine™ RNAiMAX transfection reagent and the manafacturer's protocol.

Co-immunoprecipitation and Immunoblotting Analysis

Cell pellets were resuspended in lysis buffer (100mM Tris-HCl pH 8.0, 150mM NaCl, 5% glycerol, 0.1% NP-40, 1mM DTT, 1mM AEBSF, 1µg/ml or 10µM leupeptin, 1µM pepstatin A and 1X phosphatase inhibitor). Lysates were cleared by centrifugation at 13200 RPM at 4°C for 15 minutes and normalized by measuring protein absorbance at 280nm. 10% of normalized lysates were saved for immunoblotting analysis. Pre-equilibrated Pierce™ anti-HA beads (ThermoFisher Scientific 88837) were added to the remaining normalized whole cell extracts and incubated for 30 minutes to 1 hour at 4°C by vertical rotation. Protein bound beads were washed 3 times with wash buffer (100mM Tris-HCl pH 8.0, 150mM NaCl, 5% glycerol, 0.1% NP-40, 1mM AEBSF, 1µg/ml or 10µM leupeptin, 1µM pepstatin A) and eluted for immunoblotting analysis by boiling at 95°C for 10 minutes in SDS sample loading buffer (20% glycerol, 0.01% Bromophenol Blue, 6% Sodium Dodecyl Sulfate and 120mM Tris at pH 6.8) and then reduced with 10% β-mercaptoethanol. Samples containing either whole cell extracts or anti-HA immunoprecipitants were resolved by SDS-PAGE and transferred onto PVDF membranes. Membranes were blocked with either 5% milk or 5% BSA before blotting with primary antibodies against CIAPIN1 (Santa Cruz Biotechnology sc-271298, Lot #H2317), GLRX3 (Santa Cruz Biotechnology sc-100601 Lot#C1811), CIAO3 (Santa Cruz Biotechnology sc-514078 Lot #K1914 or Sigma Aldrich SAB4502760), NUBP1 (Santa Cruz Biotechnology sc-514175, Lot #0715), NUBP2 (Proteintech 15409-1-AP), MMS19 (Proteintech 16015-1-AP or 66049-1-IG), CIAO1 (Cell Signaling 87027S Lot:1),

CIAO2B (Proteintech 20108-1-AP), CIAO2A (Proteintech 20776-1-AP), ERCC2 (Santa Cruz Biotechnology sc-101174, Lot #K0414), FTH1 (Cell Signaling #3998), FLAG (Sigma #F1804 and Proteintech), ISCU1/2 (Proteintech), HIF1α (Bethyl A300-286A), IRP2 (Santa Cruz Biotechnology sc-33682, Lot #B1116), FBXL5 (Biolegend Clone 3F5G12G9 or 10F4H9D12), GAPDH (Proteintech HRP-60004) and TUBA (Proteintech). Membranes were further blotted with HRP-labeled secondary antibodies before Pierce™ ECL Western Blotting Substrates (ThermoFisher Scientific 32106) or SuperSignal™ West Femto Maximum Sensitivity Substrate (ThermoFisher Scientific 34096) were applied. Membranes were visualized on exposed film or with the iBright™ Imaging System. Densitometric analysis of blots was carried out with ImageJ.[32]

Preparation of Peptide Standard

HEK293 cells were resuspended in lysis buffer (100mM Tris-HCl pH 8.0, 8M Urea, 1mM DTT, 1mM AEBSF, 1µg/ml or 10µM leupeptin, 1µM pepstatin A and 1x phosphatase inhibitor cocktail). Protein abundance was estimated using absorbance at 280nm. Protein solution was reduced with 5mM Tris (2-carboxyethyl) phosphine, alkylated with 10mM iodoacetamide, digested with trypsin overnight and desalted with C18 cartridge. 51µg of dried peptides were resuspended in 102µl 5% formic acid (ThermoFisher Scientific 85178) to make 500ng/µl peptide standard, which was further diluted to 250ng/µl, 125ng/µl, 62.5ng/µl with 5% formic acid.

Affinity Purification of Protein Complexes

Cell pellets from five 15cm plates were resuspended in lysis buffer (100mM Tris-HCl pH 8.0, 150mM NaCl, 5% glycerol, 0.1% NP-40, 2mM $MgCl_2$, turbo nuclease, 1mM DTT, 1mM AEBSF, 1µg/ml or 10µM leupeptin, 1µM pepstatin A). Lysates were vertically

rotated for 30 minutes at 4°C, cleared by centrifugation at 13200 RPM at 4°C for 15 minutes and normalized using protein absorbance at 280nm. 100µl of pre-equilibrated anti-HA beads (ThermoFisher Scientific 88837) or 150µl of EZview Red Anti-HA Affinity Gel (Sigma-Aldrich E6779) were added to the normalized whole cell extracts and incubated for 1 hour at 4°C by vertical rotation. Protein bound beads were washed 3 or 5 times with wash buffer (100mM Tris-HCl pH 8.0, 150mM NaCl, 5% glycerol, 0.1% NP-40, 1mM AEBSF, 1µg/ml or 10µM leupeptin, 1µM pepstatin A) and 1 or 2 additional time with clean wash buffer (100mM Tris-HCl pH 8.0, 150mM NaCl, 5% glycerol). Proteins were eluted in glycine (0.1M, pH 2). Eluates were neutralized by Tris and NaCl was added to a final concentration of 150mM. 4x volume cold acetone was used to precipitate proteins at -20°C for 2 hours or overnight. Proteins were pelleted at 15000g for 25 minutes and after discarding the supernatant, the protein pellet was washed by an additional 500µl of pure acetone. The protein pellet was dried and resuspended in digestion buffer (8M Urea in 100mM Tris pH 8.5), reduced with 5mM Tris (2-carboxyethyl) phosphine, alkylated with 10mM iodoacetamide, and digested with Lys-C and trypsin. Digestion was quenched by addition of formic acid to a final concentration of 5%. Digested peptides were desalted with C18 tip (ThermoFisher Scientific 87784) and resuspended in 5% formic acid for subsequent analysis by LC/MS.

Proteomic Characterization of Interactome

Peptides from purified protein complexes were analyzed on a Thermo Scientific™ Fusion™ Lumos™ Tribrid™ Mass Spectrometer after chromatographic separation. A Dionex™ UltiMate 3000 nanoLC system was used to deliver the chromatographic gradient onto an in-house packed 75µm by 25cm column composed of ReproSil-Pur

C18 (r119.aq.0001). Columns were washed with buffer R1 (60% acetonitrile, 20% 2-propanol and 20% water) and equilibrated in buffer A (1% 0.1% formic acid and 3% DMSO in water) before sample loading. Gradient started with 99% buffer A (1% 0.1% formic acid and 3% DMSO in water) and 1% buffer B (0.1% formic acid and 3% DMSO in acetonitrile) at a flow rate of 400nl/min. At the flow rate of 200nl/min, buffer B increased to 5.5% within the next 5 minutes, to 27.5% in the subsequent 123 minutes, to 35% in the next 7 minutes, rapidly to 80% over 1 minute, held at 80% for 2 minutes and dropped back to 1% over the next 2 minutes. A 2200V voltage was applied to ionize peptides. Samples were analyzed using data-dependent acquisition (DDA) where a full MS scan was acquired every 3 seconds at resolution of 120000 with scan range set to 400-1600 m/z. Ions with charge states between 2 to 6 and an intensity greater than 4.0e3 were selected for fragmentation by quadrupole using a 1.6 m/z isolation window. Dynamic exclusion was set at 25 seconds. MS/MS spectra were collected using 35% collision energy at a resolution of 15000.

Database Search for Identifications

MaxQuant (version 1.6.10.43 or 2.0.3.0) with the built-in Andromeda algorithm was used to search proteomic data against the EMBL-EBI Human reference proteome (UP000005640_9606, updated in April 2019) containing 20874 proteins with common contaminants appended.[33] The following search parameters were used: peptide tolerance of 20ppm for first search and 4.5ppm for main search; fragment ion tolerance of 20ppm; peptides containing fixed carbamidomethyl modification on cysteines with maximum five modifications per peptide in including variable methionine oxidation and protein N-terminus acetylation; digestion specific for trypsin and Lys-C with at most 2

missed cleavages; label free quantification was enabled as needed with only unique peptides used for quantification. False detection rates (FDRs) were evaluated through a target-decoy-based approach and filtered at 1% at both peptide spectrum match (PSM) level and protein level. MS1 level intensities from DDA experiments were calculated by MaxQuant. Changes in protein abundance were calculated using artMS with integrated MSstats package.[34,35] A linear mixed model was used to determine proteins with differential abundance.

Development and Analytical Validation of the Targeted MS Assay/Measurement for Fe-S-related Proteins.

For the targeted proteomics assay, candidate proteotypic peptides were selected from unbiased data-dependent analyses using criteria described by Rauniyar.[36] Briefly, peptides must be unique to the human proteome, 7-20 amino acids in length, and lack missed cleavage sites. Preference was also given to peptides lacking methionine, cysteine, and tryptophan which are susceptible to oxidation. These candidate peptides were then targeted using parallel reaction monitoring (PRM) in samples derived from both whole cell lysates and immunoprecipitates. Chromatography and instrument settings were identical to unbiased proteomic analyses except as indicated below. For whole cell lysate experiments, settings included an isolation window of 0.7 m/z, HCD activation with 35% collision energy, and an orbitrap resolution at 30000. Scan range mode was set to “Auto” with standard AGC target. Maximum injection time was set to “Dynamic” with at least 10 points across the peak. Data Type was set to “Centroid”. For quantification of CIAO3 interactions, settings for targeted acquisition are similar except

that isolation window was set to 1.6 m/z, maximum injection time was set to 54ms, and full MS scan was acquired.

For analysis of PRM experiments, a spectral library was first generated using PSMs from DDA acquisition of affinity purified protein complexes associated with 3HA-3FLAG-NUBP2 and His-HA-StrepII-CIAO1. Product ion chromatograms were then extracted using Skyline (20.2.0.343).[37] Extracted ion chromatograms were carefully inspected to ensure (1) co-elution of all fragment ions used for subsequent quantitation, (2) mass accuracy of the measured precursor and fragment ions relative to their theoretical masses, (3) dot product of the acquired spectra relative to its match in the spectral library, (4) differences in the observed vs expected retention times for each peptide after retention time alignment, and (5) reproducibility across multiple replicates. A high-quality list of quantotypic peptides were generated based on these data and is shown in supplemental Table S2. All PRM data used for assay validation have been added to Panorama Public with access URL https://panoramaweb.org/eGV5lu.url.

Experimental Design and Rationale

For comparative targeted experiments, two biological replicates were performed to ensure consistency of observations. Negative controls that did not contain the targeted proteins were employed to ensure specificity. Precursors with a minimum of three transitions without interferences were manually selected to generate quantitative information. MSstats, an R package developed for statistical analysis and relative quantification of mass spectrometry-based proteomics was used to determine protein abundances and significant changes across conditions.[35] Protein intensities were estimated using the summary method of Tukey's median polish and normalized to bait

protein by selecting peptides from CIAO3 as global standards. Significant changes in protein abundance were determined using a family of linear mixed-effects models. Adjusted p-values were calculated, and changes were considered significant if adjusted $P < 0.05$.

Homology Modeling of Human CIAO3

Swiss-Model was used for homology modeling of human CIAO3 based on the structure of Fe-only hydrogenase (1FEH).[31,38]

Data availability

All relevant raw files for this study have been deposited into MassIVE data repository (MassIVE MSV000088394, PXD029770, doi:10.25345/C5T85M) and Panorama Public (PXD033557).

Supporting information

This article contains supporting information.

Acknowledgements

We acknowledge members in the Wohlschlegel lab for discussion.

Author Contributions

JAW and XF designed experiments, analyzed results, and prepared the manuscript. XF, AAV, SR, and SL performed experiments and analyzed data. XF, WDB, JS, and YJ acquired proteomics data and maintained instrumentation. VP edited the manuscript.

Funding and additional information

This work was supported by the National Institutes of Health GM089778 and GM112763 to JAW. XF and WDB were additionally supported by the Ruth L. Kirschstein National Service Award from the National Institute of Health (GM007185). The content is solely

the responsibility of the authors and does not necessarily represent the official views of the National Institutes of Health.

Conflict of Interest

The authors declare that they have no conflicts of interest with the contents of this article.

References

1. Crack, J. C., Green, J., Thomson, A. J. & Le Brun, N. E. Iron-sulfur cluster sensor-regulators. *Current Opinion in Chemical Biology* **16**, 35–44 (2012).

2. Stehling, O. *et al.* MMS19 Assembles Iron-Sulfur Proteins Required for DNA Metabolism and Genomic Integrity. *Science* **337**, 195–199 (2012).

3. Ben-Shimon, L. *et al.* Fe-S cluster coordination of the chromokinesin KIF4A alters its sub-cellular localization during mitosis. *Journal of Cell Science* (2018) doi:10.1242/jcs.211433.

4. Beinert, H., Holm, R. H. & Munck, E. Iron-Sulfur Clusters: Nature's Modular, Multipurpose Structures. *Science* **277**, 653–659 (1997).

5. Maio, N. & Rouault, T. A. Outlining the Complex Pathway of Mammalian Fe-S Cluster Biogenesis. *Trends in Biochemical Sciences* **45**, 411–426 (2020).

6. Lill, R., Srinivasan, V. & Mühlenhoff, U. The role of mitochondria in cytosolic-nuclear iron-sulfur protein biogenesis and in cellular iron regulation. *Current Opinion in Microbiology* **22**, 111–119 (2014).

7. Johnson, N. B., Deck, K. M., Nizzi, C. P. & Eisenstein, R. S. A synergistic role of IRP1 and FBXL5 proteins in coordinating iron metabolism during cell proliferation. *Journal of Biological Chemistry* **292**, 15976–15989 (2017).

8. Zhu, X., Zhang, H. & Mendell, J. T. Ribosome Recycling by ABCE1 Links Lysosomal Function and Iron Homeostasis to 3' UTR-Directed Regulation and Nonsense-Mediated Decay. *Cell Reports* **32**, 107895 (2020).

9. Schwamb, B. *et al.* FAM96A is a novel pro-apoptotic tumor suppressor in gastrointestinal stromal tumors. *International Journal of Cancer* **137**, 1318–1329 (2015).

10. Kypri, E. *et al.* The nucleotide-binding proteins Nubp1 and Nubp2 are negative regulators of ciliogenesis. *Cellular and Molecular Life Sciences* **71**, 517–538 (2014).

11. Stehling, O. *et al.* Human Nbp35 Is Essential for both Cytosolic Iron-Sulfur Protein Assembly and Iron Homeostasis. *Molecular and Cellular Biology* **28**, 5517–5528 (2008).

12. Sheftel, A., Stehling, O. & Lill, R. Iron-sulfur proteins in health and disease. *Trends in Endocrinology and Metabolism* **21**, 302–314 (2010).

13. Fuss, J. O., Tsai, C. L., Ishida, J. P. & Tainer, J. A. Emerging critical roles of Fe-S clusters in DNA replication and repair. *Biochimica et Biophysica Acta - Molecular Cell Research* **1853**, 1253–1271 (2015).

14. Patel, S. J. *et al.* A PCBP1–BolA2 chaperone complex delivers iron for cytosolic [2Fe–2S] cluster assembly. *Nature Chemical Biology* **15**, 872–881 (2019).

15. Netz, D. J. A., Pierik, A. J., Stümpfig, M., Mühlenhoff, U. & Lill, R. The Cfd1-Nbp35 complex acts as a scaffold for iron-sulfur protein assembly in the yeast cytosol. *Nature Chemical Biology* **3**, 278–286 (2007).

16. Gari, K. *et al.* MMS19 Links Cytoplasmic Iron-Sulfur Cluster Assembly to DNA Metabolism. **3801**, 2011–2013 (2012).

17. Frey, A. G., Palenchar, D. J., Wildemann, J. D. & Philpott, C. C. A glutaredoxin-BolA complex serves as an iron-sulfur cluster chaperone for the cytosolic cluster assembly machinery. *Journal of Biological Chemistry* **291**, 22344–22356 (2016).

18. Vashisht, A. A., Yu, C. C., Sharma, T., Ro, K. & Wohlschlegel, J. A. The association of the xeroderma pigmentosum group D DNA helicase (XPD) with

transcription factor IIH is regulated by the cytosolic iron-sulfur cluster assembly pathway. *Journal of Biological Chemistry* **290**, 14218–14225 (2015).

19. Meyron-Holtz, E. G., Ghosh, M. C. & Rouault, T. A. Mammalian tissue oxygen levels modulate iron-regulatory protein activities in vivo. *Science* **306**, 2087–2090 (2004).

20. Vashisht, A. A. *et al.* Control of Iron Homeostasis by an Iron-Regulated Ubiquitin Ligase. *Science* **326**, 718–721 (2009).

21. Golinelli, M. P., Chmiel, N. H. & David, S. S. Site-directed mutagenesis of the cysteine ligands to the [4Fe-4S] cluster of Escherichia coli MutY. *Biochemistry* **38**, 6997–7007 (1999).

22. Seki, M., Takeda, Y., Iwai, K. & Tanaka, K. IOP1 protein is an external component of the human cytosolic iron-sulfur cluster assembly (CIA) machinery and functions in the MMS19 protein-dependent CIA pathway. *Journal of Biological Chemistry* **288**, 16680–16689 (2013).

23. Kim, K. S., Maio, N., Singh, A. & Rouault, T. A. Cytosolic HSC20 integrates de novo iron-sulfur cluster biogenesis with the CIAO1-mediated transfer to recipients. *Human Molecular Genetics* **27**, 837–852 (2018).

24. Carr, S. A. *et al.* Targeted peptide measurements in biology and medicine: Best practices for mass spectrometry-based assay development using a fit-for-purpose approach. *Molecular and Cellular Proteomics* **13**, 907–917 (2014).

25. Trotta, R. J., Sullivan, S. G. & Stern, A. Lipid peroxidation and haemoglobin degradation in red blood cells exposed to t-butyl hydroperoxide. The relative roles of haem- and glutathione-dependent decomposition of t-butyl hydroperoxide and

membrane lipid hydroperoxides in lipid peroxidation and ha. *Biochemical Journal* **212**, 759–772 (1983).

26. Martinez, M. T. P. *et al.* Mechanisms of iron- and O2-sensing by the [4Fe-4S] cluster of the global iron regulator RirA. *eLife* **8**, 1–26 (2019).

27. Balk, J., Pierik, A. J., Aguilar Netz, D. J., Mühlenhoff, U. & Lill, R. The hydrogenase-like Nar1p is essential for maturation of cytosolic and nuclear iron-sulphur proteins. *EMBO Journal* **23**, 2105–2115 (2004).

28. Maione, V., Grifagni, D., Torricella, F., Cantini, F. & Banci, L. CIAO3 protein forms a stable ternary complex with two key players of the human cytosolic iron–sulfur cluster assembly machinery. *Journal of Biological Inorganic Chemistry* **25**, 501–508 (2020).

29. Urzica, E., Pierik, A. J., Mühlenhoff, U. & Lill, R. Crucial role of conserved cysteine residues in the assembly of two iron-sulfur clusters on the CIA protein Nar1. *Biochemistry* **48**, 4946–4958 (2009).

30. Liu, H. Z. *et al.* A novel mutation in nuclear prelamin a recognition factor-like causes diffuse pulmonary arteriovenous malformations. *Oncotarget* **8**, 2708–2718 (2017).

31. Peters, J. W., Lanzilotta, W. N., Lemon, B. J. & Seefeldt, L. C. X-ray Crystal Structure of the Fe-Only Hydrogenase (CpI) from Clostridium pasteurianum to 1.8 Angstrom Resolution. *Science* **282**, 1853–1858 (1998).

32. Schneider, C. A., Rasband, W. S. & Eliceiri, K. W. NIH Image to ImageJ: 25 years of image analysis. *Nature Methods* **9**, 671–675 (2012).

33. Tyanova, S., Temu, T. & Cox, J. The MaxQuant computational platform for mass spectrometry-based shotgun proteomics. *Nature Protocols* **11**, 2301–2319 (2016).

34. Jimenez-Morales, D., Campos, A. R., Von Dollen, J., Krogan, N. & Swaney, D. artMS: Analytical R tools for Mass Spectrometry. (2021).

35. Choi, M. *et al.* MSstats: An R package for statistical analysis of quantitative mass spectrometry-based proteomic experiments. *Bioinformatics* **30**, 2524–2526 (2014).

36. Rauniyar, N. Parallel Reaction Monitoring: A Targeted Experiment Performed Using High Resolution and High Mass Accuracy Mass Spectrometry. *Int J Mol Sci* **16**, 28566-28581 (2015).

37. MacLean, B. *et al.* Skyline: An open source document editor for creating and analyzing targeted proteomics experiments. *Bioinformatics* **26**, 966–968 (2010).

38. Waterhouse, A. *et al.* SWISS-MODEL: Homology modelling of protein structures and complexes. *Nucleic Acids Research* **46**, W296–W303 (2018).

Abbreviations and Nomenclature

CIA: cytosolic iron-sulfur cluster assembly

ISC: mitochondrial iron-sulfur cluster assembly

ROS: reactive oxygen species

MMS19: MMS19 nucleotide excision repair protein homolog

CIAO1: probable cytosolic iron-sulfur protein assembly protein CIAO1

CIAO2B: cytosolic iron-sulfur assembly component 2B

CIAO3: cytosolic iron-sulfur assembly component 3

NUBP1: nucleotide-binding protein 1

NUBP2: nucleotide-binding protein 2

Figures and figure legends

Figure 2-1. CIA components and substrates form higher order complexes.

(A) HEK293 cells were treated with 100μg/ml ammonium ferric citrate (FAC) or 100μM deferoxamine (DFO) for 8 hours to create an iron sufficient or deficient environment, respectively. Whole cell extracts (WCE) were resolved by SDS-PAGE and blotted with antibodies against known components of the cytosolic iron-sulfur cluster assembly (CIA) pathway, CIA substrates, loading control α-tubulin, FAC treatment control FBXL5 and DFO treatment control IREB2.

(B) Flp-In^{TM} T-Rex^{TM} 293 cell line (Flp-In 293) engineered to stably express NUBP2 was induced overnight with 1μg/ml doxycycline. Affinity purified NUBP2 and associated proteins were identified by bottom-up proteomics. Data-dependent acquisition of two technical replicates was performed. Spectra count (SpC) for selected proteins combined from the two technical replicates were shown.

(C) Parallel reaction monitoring was conducted on HEK293 whole cell lysate with indicated amounts of protein using a targeted proteomics assay that monitors the abundance of known CIA factors (ABCB7, GLRX3, BOLA2, CIAPIN1, NUBP1, NUBP2, CIAO3, CIAO1, CIAO2B, CIAO2A, MMS19) and prototypical substrates (CDKAL1, DNA2, ERCC2, POLD1 and ABCE1). Two technical replicates were acquired. Intensities were normalized for each precursor to the highest intensity in a replicate.

(D) Flp-In 293 cells that stably express NUBP2 were induced with 1μg/ml doxycycline. Affinity purified NUBP2 and associated proteins were identified by acquisition of a targeted proteomic assay containing CIA scaffold complex components (NUBP1 and NUBP2), CIAO3, CIA targeting complex components (MMS19, CIAO1 and CIAO2B)

and prototypical substrates (CDKAL1, DNA2, ERCC2, POLD1 and ABCE1). Two biological replicates were performed. Acquired spectra were searched with MaxQuant. Each edge represents a peptide identified. Solid edges connect bait protein to known interactors while dashed edges connect to novel interactors discovered in our study. Edge widths correspond to the posterior error probability (PEP) of each peptide.

(E) Flp-In 293 background cells or cells expressing NUBP2 were either directly harvested or after treatment with 1% formaldehyde. Anti-HA immunoprecipitation were performed. WCEs and anti-HA immunoprecipitates were blotted for CIAO3, CIA targeting complex components and the CIA substrate CDKAL1.

Figure 2-1

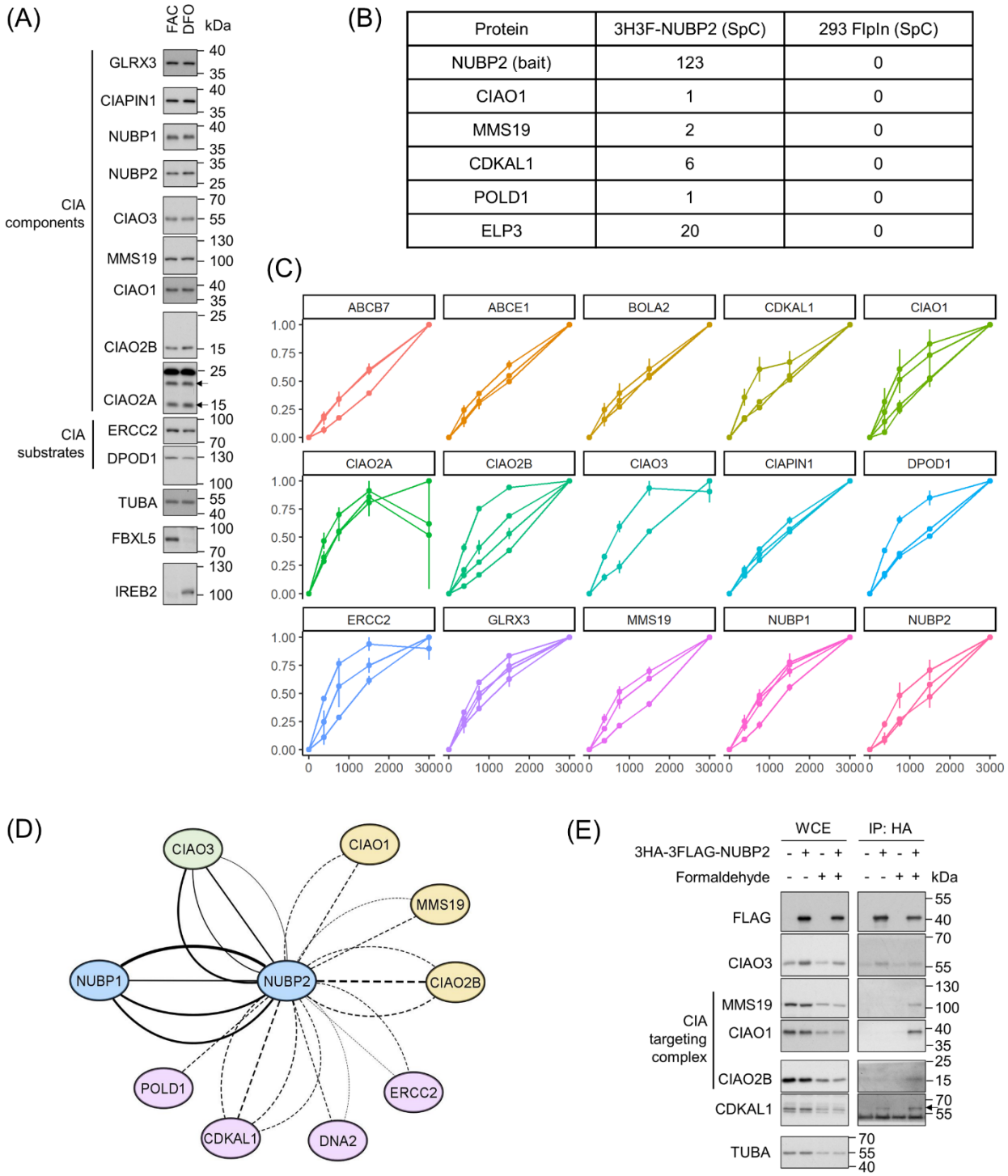

Protein	3H3F-NUBP2 (SpC)	293 FlpIn (SpC)
NUBP2 (bait)	123	0
CIAO1	1	0
MMS19	2	0
CDKAL1	6	0
POLD1	1	0
ELP3	20	0

Figure 2-2. CIAO3 interactions are regulated by intracellular iron level in a time-dependent manner.

(A, B and C) Flp-In 293 stably expressing 3HA-3FLAG tagged CIAO3 was induced with 1μg/ml doxycycline for 24 hours and treated with 100μg/ml FAC or 100μM DFO for 8 hours before harvesting. Two biological replicates were performed for each experiment. (A) Affinity purified CIAO3 and associated proteins were characterized by shotgun proteomics and quantified by MS1 intensity-based label-free quantification. Abundance of co-eluted (B) CIA scaffold complex components (NUBP1 and NUBP2) and (C) CIA targeting complex components (MMS19, CIAO1 and CIAO2B) were monitored using a targeted proteomic assay. Log2 of calculated protein intensities (Log2Intensities) under FAC or DFO condition were plotted with mean ± SD. * denotes $P<0.05$.

(D) Flp-In 293 cells or Flp-In 293 expressing NUBP2 were induced with 1μg/ml doxycycline for 24 hours. Cells expressing 3HA-3FLAG-NUBP2 were treated with 100μg/ml FAC, untreated or treated with 100μM DFO for 8 hours before harvesting. WCEs and anti-HA immunoprecipitates (IP: HA) were analyzed by immunoblotting with antibodies against FLAG, CIAO3, loading control α-tubulin and FAC/DFO treatment control FTH1.

(E) Flp-In 293 background cells or cells stably expressing 3HA-3FLAG-CIAO3 were induced with 1μg/ml doxycycline overnight, untreated or treated with 100μg/ml FAC or 100μM DFO for hours indicated. WCEs and anti-HA immunoprecipitates (IP: HA) were blotted with antibodies against indicated proteins.

Figure 2-2

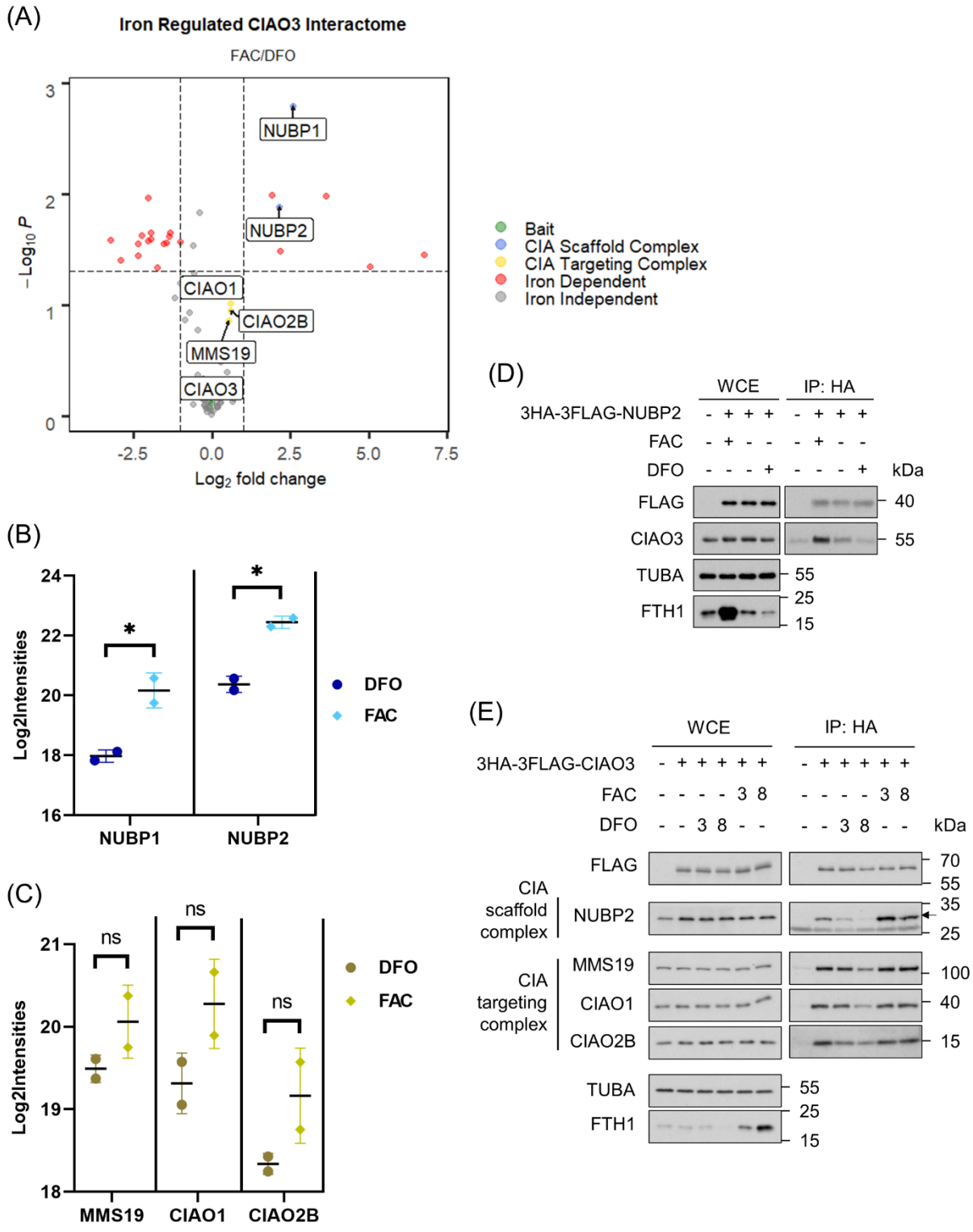
(A)
Iron Regulated CIAO3 Interactome
FAC/DFO
NUBP1
NUBP2
CIAO1
CIAO2B
MMS19
CIAO3
−Log10 P
Log2 fold change
Bait
CIA Scaffold Complex
CIA Targeting Complex
Iron Dependent
Iron Independent
(B)
Log2Intensities
DFO
FAC
NUBP1
NUBP2
(C)
Log2Intensities
ns
DFO
FAC
MMS19
CIAO1
CIAO2B
(D)
WCE
IP: HA
3HA-3FLAG-NUBP2
FAC
DFO
kDa
FLAG
CIAO3
TUBA
FTH1
40
55
55
25
15
(E)
WCE
IP: HA
3HA-3FLAG-CIAO3
FAC
DFO
kDa
FLAG
CIA scaffold complex
NUBP2
CIA targeting complex
MMS19
CIAO1
CIAO2B
TUBA
FTH1
70
55
35
25
100
40
15
55
25
15

Figure 2-3. CIAO3 interactions are altered by changes in cellular redox state and requires functional mitochondrial Fe-S cluster biogenesis.

(A) Flp-In 293 cells expressing 3HA-3FLAG-CIAO3 were treated with tert-Butyl hydroperoxide (tBHP) for 4 hours to introduce reactive oxygen species. WCEs and anti-HA immunoprecipitates were blotted with antibodies against indicated proteins and loading control GAPDH.

(B) Flp-In 293 cells expressing 3HA-3FLAG-CIAO3 or control cells were induced with 1μg/ml doxycycline overnight and cultured in 21% O_2 or 1% O_2 for 16 hours before harvesting. WCEs and anti-HA immunoprecipitates were immunoblotted with antibodies against NUBP2, loading control α-tubulin and hypoxia treatment control HIF1α.

(C) Mitochondrial iron-sulfur cluster biogenesis was disrupted by using siRNA to silence ISCU1/2 in Flp-In 293 cells for 48 hours while control cells were treated with non-target siRNA. Doxycycline was added to induce expression of 3HA-3FLAG-CIAO3. WCEs and HA immunoprecipitates were blotted with indicated antibodies.

(D and E) Quantification of (C) by densitometry. Protein abundance of coimmunoprecipitated proteins were normalized to the protein level of immunoprecipitated bait (3HA-3FLAG-CIAO3). Mean ± SD was plotted for n = 3 independent experiments. *P<0.05, **P<0.01.

Figure 2-3

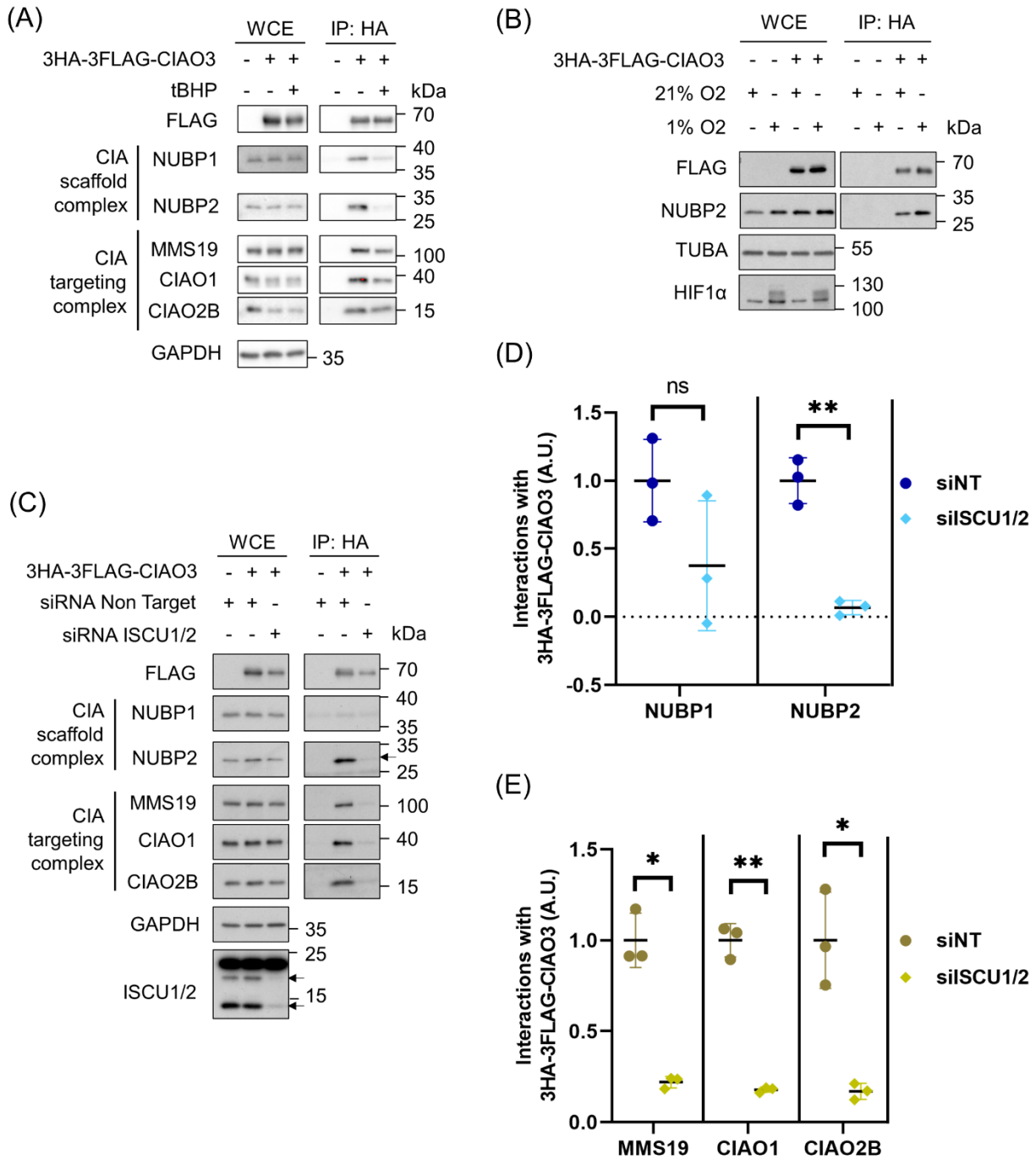
(A)
WCE
IP: HA
3HA-3FLAG-CIAO3
tBHP
kDa
FLAG
CIA scaffold complex
NUBP1
NUBP2
CIA targeting complex
MMS19
CIAO1
CIAO2B
GAPDH
(B)
21% O2
1% O2
TUBA
HIF1α
(C)
siRNA Non Target
siRNA ISCU1/2
ISCU1/2
(D)
ns
Interactions with 3HA-3FLAG-CIAO3 (A.U.)
siNT
siISCU1/2
(E)

Figure 2-4. Fe-S cluster incorporation into CIAO3 controls its interactions.

(A) Schematic representation of Fe-S incorporation in wild-type CIAO3 and mutants.

(B, C and D) Flp-In 293 cells that stably express wild-type or mutant CIAO3 were induced with 1 μg/ml doxycycline for 24 hours before harvesting. CIAO3 and associated proteins were affinity purified. Two biological replicates were analyzed. Protein abundances were monitored by a targeted proteomic assay containing known CIA components and a subset of prototypical CIA substrates after normalization to CIAO3 levels. Log2 transformed abundance of the co-eluted proteins (Log2Intensiteis) were plotted for the CIA scaffold complex (B), the CIA targeting complex (C), and selected CIA substrates (D). Mean ± SD was indicated. Protein levels of interactors co-eluted with mutant CIAO3 were compared to wild type. *P<0.05, **P<0.01, ***P<0.001 and ****P<0.0001.

(E) Flp-In 293 control cells, cells expressing wild-type 3HA-3FLAG-ERCC2, and cells expressing mutant ERCC2 lacking the MMS19 binding region were induced with 1μg/ml doxycycline for 24 hours. Cell lysates were immunoprecipitated. WCEs and HA immunoprecipitates were blotted with indicated antibodies.

Figure 2-4.

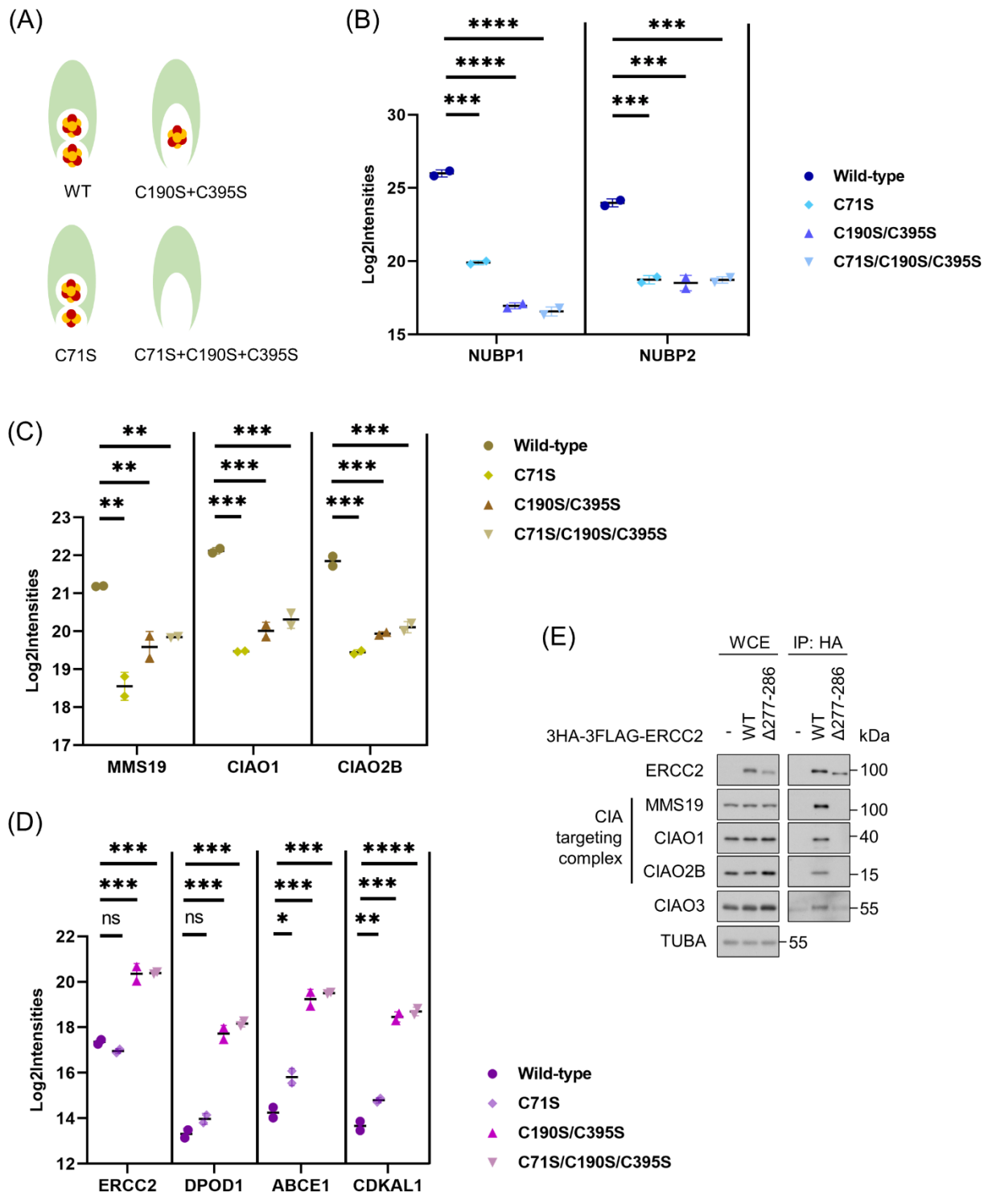
(A)
WT
C190S+C395S
C71S
C71S+C190S+C395S
(B)
Log2Intensities
NUBP1
NUBP2
Wild-type
C71S
C190S/C395S
C71S/C190S/C395S
(C)
Log2Intensities
MMS19
CIAO1
CIAO2B
(D)
Log2Intensities
ERCC2
DPOD1
ABCE1
CDKAL1
ns
(E)
WCE
IP: HA
3HA-3FLAG-ERCC2
WT
Δ277-286
kDa
ERCC2
MMS19
CIAO1
CIAO2B
CIAO3
TUBA
CIA targeting complex

Figure 2-5. CIAO3 mutant associated with PAVMs cannot assemble into the higher order complexes.

(A) Homology modelled human CIAO3 from iron-only hydrogenase (1FEH) showing distances from Serine 161 to Proline or to the C-terminal Fe-S cluster.

(B) Sequence alignment of CIAO3 orthologs.

(C) WCEs and HA immunoprecipitates from Flp-In 293 cells expressing wildtype CIAO3, the S161I mutant, or control cells were analyzed by SDS-PAGE and immunoblotted with antibodies indicated.

(D, E and F) Quantification of (C) by densitometry showing baseline corrected protein abundance of coimmunoprecipitated proteins with respect to the bait protein (3HA-3FLAG-CIAO3 wild-type or S161I). Mean ± SD was plotted for n = 3 independent experiments. *P<0.05.

Figure 2-5.

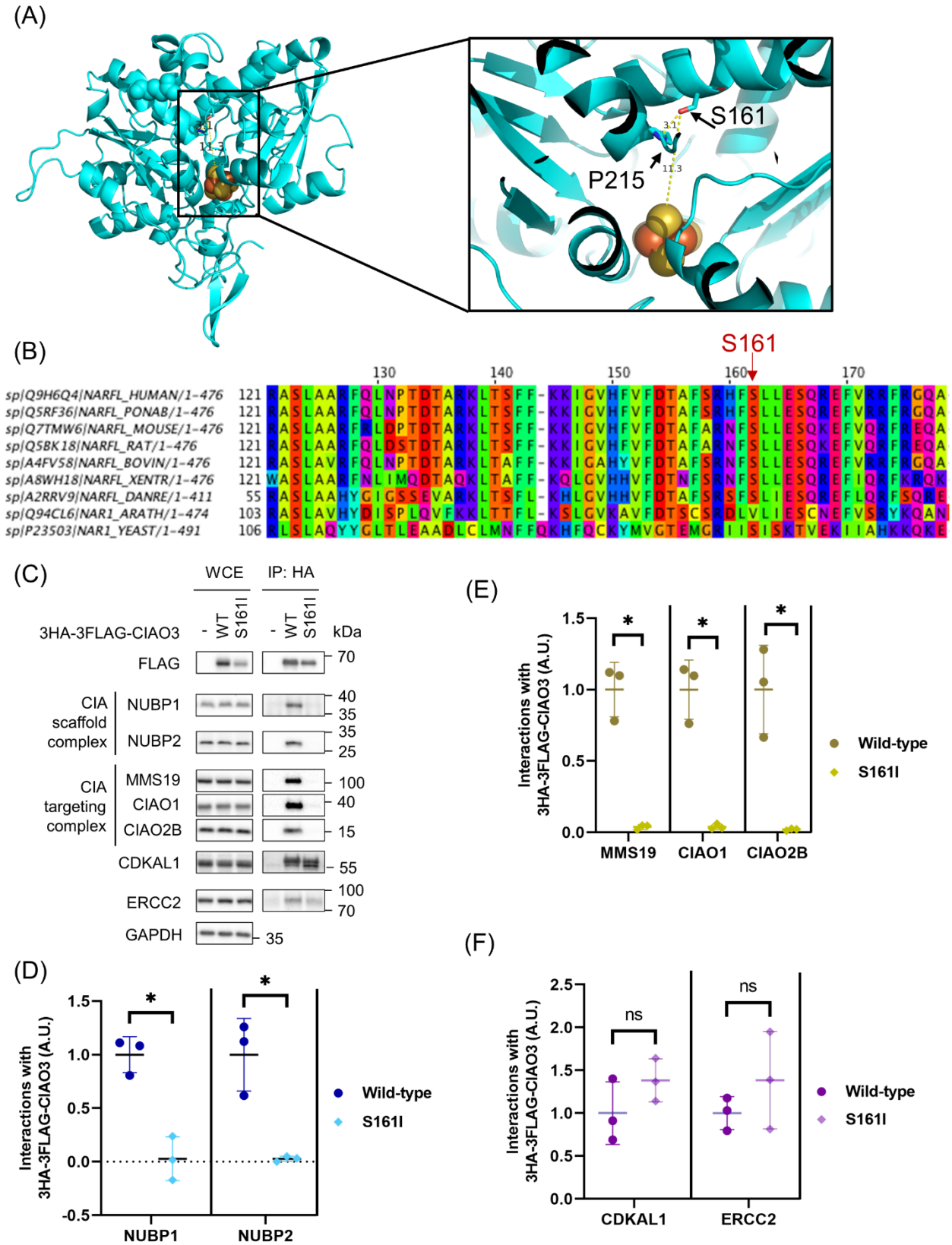
(A)
S161
P215
(B)
S161
sp|Q9H6Q4|NARFL_HUMAN/1-476
sp|Q5RF36|NARFL_PONAB/1-476
sp|Q7TMW6|NARFL_MOUSE/1-476
sp|Q5BK18|NARFL_RAT/1-476
sp|A4FV58|NARFL_BOVIN/1-476
sp|A8WH18|NARFL_XENTR/1-476
sp|A2RRV9|NARFL_DANRE/1-411
sp|Q94CL6|NAR1_ARATH/1-474
sp|P23503|NAR1_YEAST/1-491
(C)
WCE
IP: HA
3HA-3FLAG-CIAO3
WT
S161I
kDa
FLAG
CIA scaffold complex
NUBP1
NUBP2
CIA targeting complex
MMS19
CIAO1
CIAO2B
CDKAL1
ERCC2
GAPDH
(D)
Interactions with 3HA-3FLAG-CIAO3 (A.U.)
NUBP1
NUBP2
Wild-type
S161I
(E)
Interactions with 3HA-3FLAG-CIAO3 (A.U.)
MMS19
CIAO1
CIAO2B
Wild-type
S161I
(F)
Interactions with 3HA-3FLAG-CIAO3 (A.U.)
ns
CDKAL1
ERCC2
Wild-type
S161I

Figure 2-6. Model for the regulated assembly of the CIA machinery in response to ROS, O_2 tension, intracellular iron levels, and Fe-S cluster assembly on CIAO3.

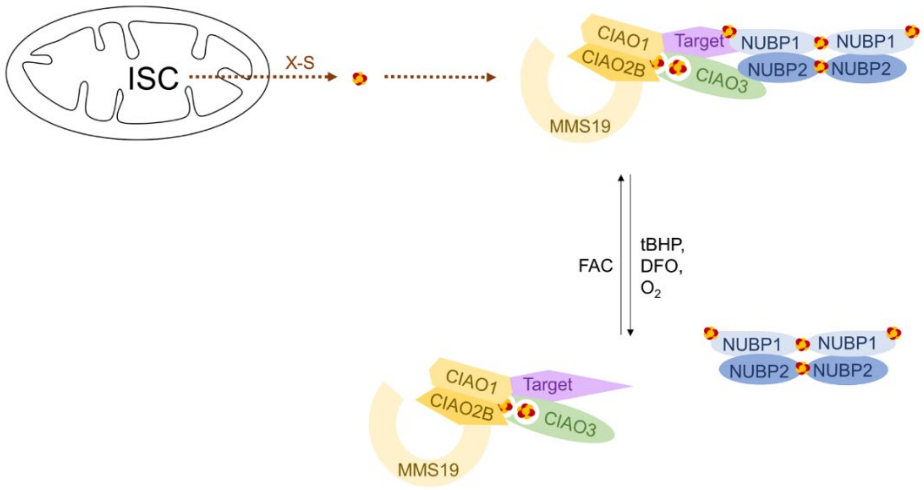

Table 2-1 List of monitored peptides. (Related to Fig. 2-1C, 2-1D, 2-2B and 2-4B to 2-4D). This list includes mass-to-charge and charge of all precursors monitored. In the experiment identifying proteins that are associate NUBP2 (Fig. 2-1D), a subset of precursors was monitored to increase the sensitivity for the CIA targeting complex and substrates.

Precursors	m/z	z	Protein
LQEEIVNSVK	579.8219	2	ABCB7
AGAAFFNEVR	541.2749	2	ABCB7
TSIFIAHR	472.7693	2	ABCB7
GQSFFIDAPDSPATLAYR	978.4785	2	NUBP1
VPLDPLIGK	476.2973	2	NUBP1
DVDWGEVDYLIVDTPPGTSDEHLSVVR	1005.1524	3	NUBP1
LCASGAGATPDTAIEEIK	902.4433	2	NUBP1
GWAPVFLDR	530.7824	2	NUBP2
STISTELALALR	637.8694	2	NUBP2
TLEEGHDFIQEFPGSPAFAALTSIAQK	968.8187	3	NUBP2
HIILVLSGK	490.3186	2	NUBP2
ELQREPLTPEEVQSVR	637.3374	3	CIAPIN1
SSPSVKPAVDPAAAK	712.8908	2	CIAPIN1
SACGNCYLGDAFR	745.8112	2	CIAPIN1
KPDPASLR	442.2534	2	CIAPIN1
DLEAEHVEVEDTTLNR	623.9657	3	BOLA2
DLEAEHVEVEDTTLNR	935.4449	2	BOLA2
TLTPDQWAR	544.2802	2	BOLA2
LVNACLAEELPHIHAFEQK	740.3808	3	BOLA2
AYSNWPTYPQLYVK	865.4329	2	GLRX3
GELVGGLDIVK	550.3215	2	GLRX3

LEAEGVPEVSEK	643.8274	2	GLRX3
ELPQVSFVK	523.7977	2	GLRX3
FTLLFLQEAPSTGSEGQR	991.0049	2	NDOR1
ELGSLVWELLDR	715.3879	2	NDOR1
VTGPSHFQDVR	621.8149	2	NDOR1
LVVVSVSPQSR	585.8457	2	CIAO3
GGGSGGYLEHVFR	668.3257	2	CIAO3
DFFAQQQHLTPDK	787.8835	2	CIAO3
LLHTQYHAVEK	446.9103	3	CIAO3
DVDCVLTTGEVFR	755.863948	2	CIAO3
HFSLLESQR	558.7935	2	CIAO3
LEALQESLPPALHGSR	573.3126	3	NARF
EVLHTTYQSQER	745.8653	2	NARF
LLQAAAGASAR	514.796	2	MMS19
EVFQTASER	533.7618	2	MMS19
LDSLQTLNACCAVYGQK	970.963868	2	MMS19
FLNLSSSPSMAVR	704.866294	2	MMS19
HPAGQQLDEFLQLAVDK	636.9987	3	MMS19
VDSEVLSAK	474.2558	2	MMS19
FAEFLLPLLIEK	716.9261	2	MMS19
DSLVLLGR	436.7636	2	CIAO1
HVVWHPSQELLASASYDDTVK	596.2986	4	CIAO1
YQRPEGL	431.7245	2	CIAO1
SVLSEGHQR	506.7622	2	CIAO1
SGERPVTAGEEDEQVPDSIDAR	1179.0462	2	CIA2B
SGERPVTAGEEDEQVPDSIDAR	786.3666	3	CIA2B
EIFDLIR	453.2582	2	CIA2B
SINDPEHPLTLEELNVVEQVR	811.087	3	CIA2B
ALEVYDLIR	546.3084	2	CIA2A

VSGLLSWTLSR	609.8457	2	CIA2A
VLWLSGLSEPGAAR	728.4014	2	CIA2A
LEIYISEGTHSTEEDINK	693.3357	3	CIA2A
IFEPILGEGR	565.8139	2	DPOD1
SEGGEDYTGATVIEPLK	883.4282	2	DPOD1
VTGVPLSYLLSR	652.8823	2	DPOD1
NVEDLSGGELQR	658.8257	2	ABCE1
AIIKPQYVDQIPK	504.9643	3	ABCE1
VIVFDGVPSK	530.8055	2	ABCE1
ENDFLTFDAMR	679.8059	2	ERCC2
GAILLSVAR	450.2873	2	ERCC2
FYEEFDAHGR	424.1878	3	ERCC2
FQSVIITSGTLSPLDIYPK	1040.0723	2	ERCC2
GLSIIGVQQIDR	649.875	2	CDKAL1
IVLAGCVPQAQPR	704.8901	2	CDKAL1
NGLGNQLSSGSHTSAASQCDSASSR	827.0336	3	CDKAL1
QQVLVTEESFDSK	755.3752	2	CDKAL1
VVEVVEETIK	572.8266	2	CDKAL1
VFHSYSPYDHK	460.5508	3	CDKAL1
YLVLAVNTVQNK	681.393	2	DNA2
TQLASLPQIIEEEK	799.9354	2	DNA2
SGSCIGNLIR	538.7795	2	DNA2
SPGPFFSTR	498.2509	2	RTEL1
GVIVTGLPYPPR	634.8717	2	RTEL1
LVSHPEEPVAGAQTDR	569.2883	3	RTEL1
SLDLHVPSLK	554.8217	2	RTEL1
AQPVLDPTGR	527.288	2	RTEL1

Table 2-2. Proteins detected by parallel reaction monitoring in NUBP2 and background immunoprecipitates. (Related to Fig. 2-1D). NUBP2 immunoprecipitate or immunoprecipitate from background cells were subject to analysis by parallel reaction monitoring. Precursors monitored were provided in Table 2-1. Two biological replicates were analyzed. The table includes peptides identified and Q-value of each protein.

Protein	Q-value	Peptide sequences
CIAO1	0	DSLVLLGR SVLSEGHQR
ERCC2	0	AVIMFGVPYVYTQSR FQSVIITSGTLSPLDIYPK
POLD1	0	SEGGEDYTGATVIEPLK
DNA2	0	TQLASLPQIIEEEK YLVLAVNTVQNK
NUBP1	0	DVDWGEVDYLIVDTPPGTSDEHLSVVR GQSFFIDAPDSPATLAYR LCASGAGATPDTAIEEIK VPLDPLIGK
CDKAL1	0	GLSIIGVQQIDR IVLAGCVPQAQPR NGLGNQLSSGSHTSAASQCDSASSR QQVLVTEESFDSK
MMS19	0	HPAGQQLDEFLQLAVDK LLQAAAGASAR
CIAO3	0	DFFAQQQHLTPDK GGGSGGYLEHVFR LLHTQYHAVEK LVVVSVSPQSR
CIAO2B	0	EIFDLIR SGERPVTAGEEDEQVPDSIDAR SINDPEHPLTLEELNVVEQVR
NUBP2	0	GWAPVFLDR HIILVLSGK STISTELALALR TLEEGHDFIQEFPGSPAFAALTSIAQK

Table 2-3. Iron-regulated CIAO3 interactions. (Related to Fig. 2-2A). Flp-In 293 cells stably expressing 3HA-3FLAG tagged CIAO3 or background cells were treated with either FAC or DFO to stimulate a high or low iron environment. Anti-HA immunoprecipitation was performed and tryptic-digested immunoprecipitates were analyzed by data-dependent acquisition followed by intensity-based label-free quantification. The MSstats comparison of CIAO3-interacting proteins between the high and low iron conditions was also provided. This data was used for plotting Fig. 2-2A. Proteins were omitted from the list that were not significantly enriched for interacting with CIAO3.

Protein	imputed	iLog2FC	iPvalue
TMEM132D	yes	6.749289187	0.0355988
PRICKLE2	yes	5.025944317	0.0452652
CYP24A1	yes	3.651178685	0.0104116
NUBP1	no	2.589185393	0.001628785
LBR	yes	2.187221159	0.0325065
NUBP2	no	2.158611825	0.013057596
PTCD2	yes	1.913652398	0.0101607
MYBBP1A	no	0.694710123	0.706324466
LLPH	no	0.647923406	0.740834985
CIAO1	no	0.610417082	0.096377486
CIAO2B	no	0.586729879	0.113032747
MMS19	no	0.533990109	0.140062115
HP	no	0.471358597	0.402259134
ZNF664	no	0.32094615	0.59817284
PLK1	no	0.288186712	0.749529989
LDHB	no	0.277370857	0.758151531

OAT	no	0.266079341	0.32869722
SDHA	no	0.212270824	0.567376833
C1QBP	no	0.199343204	0.829793822
RPL34	no	0.170837957	0.82886825
ERAL1	no	0.170356371	0.612694205
GCN1	no	0.149193092	0.73744935
NDUFB10	no	0.146693718	0.821685737
UTS2	no	0.048961973	0.893455888
PLBD2	no	-0.017277116	0.962276275
CIAO3	no	-0.018871281	0.776000723
HSPA5	no	-0.046879164	0.9027542
NUBPL	no	-0.047365063	0.304227977
ERCC2	no	-0.067540121	0.842413474
RAB6B	no	-0.070984681	0.827383675
MICU1	no	-0.082267935	0.742275285
CLK3	no	-0.092370317	0.75544236
ELSPBP1	no	-0.15287438	0.916532266
HSPA6	no	-0.160645897	0.668283758
RAF1	no	-0.170653186	0.632652646
COX4I1	no	-0.180733092	0.840931041
MDK	no	-0.18735747	0.846106654
HSPB1	no	-0.213792287	0.799568267
LPCAT1	no	-0.236999873	0.801665701
LTV1	no	-0.252666447	0.695918888
ATP6V1H	no	-0.264001021	0.500593795
DNAJC9	no	-0.26840726	0.706733586
SFRP1	no	-0.282045491	0.613361487
HSPA1A	no	-0.290784104	0.459831593
SLC1A5	no	-0.294216359	0.680224111

NOL6	no	-0.393156985	0.014832871
HSPA8	no	-0.449916318	0.430008717
GMDS	no	-0.452812595	0.168123234
CCT5	no	-0.471404034	0.310209524
ATP1A1	no	-0.545566474	0.474459403
GLUD1	no	-0.573235352	0.05192596
MSI1	no	-0.579623654	0.294089654
DDB1	no	-0.589622034	0.029122468
NME2	no	-0.592567891	0.787001981
UBTF	no	-0.676871619	0.29433144
TUBB8	no	-0.706718709	0.116024921
POLR2B	no	-0.868507331	0.135853912
CHTOP	yes	-1.008983263	0.0272222
TUBB4A	no	-1.016439467	0.063053817
CBWD1	no	-1.18268026	0.086207779
CCAR2	yes	-1.315151749	0.0224422
PPAT	yes	-1.359098955	0.0243232
PGM3	yes	-1.450491836	0.0276052
PDHA1	yes	-1.534227557	0.0278241
TMPO	yes	-1.741534825	0.046471
TRIM28	yes	-1.929057658	0.0222598
AQR	yes	-1.949742318	0.0256602
ARAF	yes	-2.021354402	0.010753
ELP3	yes	-2.038232736	0.0267386
PRDX4	yes	-2.237629622	0.0235047
P01893	yes	-2.346989011	0.0282545
HNRNPA3	yes	-2.359446118	0.0356883
RALY	yes	-2.899450593	0.0392262
MLF2	yes	-3.231789423	0.0261987

CHAPTER 3

Exploring the Architecture of the Cytosolic Iron-Sulfur Cluster Assembly Targeting Complex with Crosslinking Mass Spectrometry

Introduction

Iron-sulfur (Fe-S) clusters are cofactors discovered throughout bacteria, archaea and eukaryotes.[1] In eukaryotes, the biogenesis of these clusters is compartmentalized, with the cytosolic iron-sulfur cluster assembly (CIA) pathway mediating the cluster incorporation into cytosolic and nuclear Fe-S proteins.[2] The CIA targeting complex consists of CIA proteins MMS19, CIAO1 and CIAO2B.[3,4] There are over 30 common interactors of these CIA proteins, among which a progressively increasing portion has been confirmed to bind Fe-S clusters.[3,5–7] Silencing components of the CIA targeting complex disrupts the Fe-S cluster acquisition by these interactors, leading to reduced stability and improper localization of these Fe-S proteins.

Although the number of identified extramitochondrial Fe-S proteins is rapidly increasing, it remains ambiguous how the CIA targeting complex recognizes this wide range of recipient proteins and facilitates the substrate maturation. In recent years, several studies have attempted to answer this question by determining the spatial organization of the CIA targeting complex. These efforts started by investigating binary interactions of CIA components and substrates. However, the conclusions reached by two independent studies were contradictory.[8,9] While one study suggested that MMS19 was associated with CIAO1 through CIAO2B, the other suggested that MMS19 directly bound to CIAO1 but not CIAO2B. The conflicts of these two studies further extended to the subunit responsible for substrate binding. These disagreements were addressed by the *in vitro* characterization of the yeast CIA targeting complex, which illustrated that CIAO2B bridged MMS19 and CIAO1, and that CIAO2B-CIAO1 resided at the C-terminus of MMS19.[10] More recently, the structure was solved of the reconstituted CIA

targeting complex from mouse MMS19, drosophila CIAO1 and drosophila CIAO2B.[11] The author confirmed the architecture of the CIA targeting complex that CIAO1 binds MMS19 at its C-terminus via CIAO2B. In addition, the author revealed two substrate binding sites in the CIA targeting complex, one at blade 3 of CIAO1 and the other at the N-terminus of MMS19.

With great technical advances in recent years, the application of crosslinking mass spectrometry (XL-MS) in structural biology has been emerging for mapping interacting surfaces, probing conformational changes, and complementing other structural biology methods by providing distance restraints and the orientation of interactions. Here, we reported our work in testing the XL-MS workflow and exploring the architecture of the CIA targeting complex.

Results

Crosslinking mass spectrometry of the CIA targeting complex – In order to obtain the CIA targeting complex, we generated HEK293 cells stably expressing N-terminal His6-HA-StrepII (HHS) tagged MMS19. We performed tandem purification using Strep-Tactin Sepharose followed by Ni-NTA (Fig. 3-1A). A small portion of purified protein complexes bound to the Ni bead was analyzed by mass spectrometry. The proteins identified with the highest abundance were MMS19, CIAO2B and CIAO1, which are all the components of the CIA targeting complex (Fig. 3-1B). CIA substrates were also copurified with MMS19 such as DNA primase (PRIM1 and PRIM2) and CDKAL1. Purified protein complexes were aliquoted and titrated with different concentrations of the lysine targeting crosslinker disuccinimidyl suberate (DSS), and the optimal concentration of DSS was determined by the disappearance of monomeric HHS-

MMS19 (Fig. 3-1C). Crosslinked protein complexes were digested and analyzed. We were able to identify 154 crosslinked peptides with 706 crosslinked spectra. These included crosslinks between the C-terminus of MMS19 with CIAO2B, which is consistent with the structure of the reconstituted CIA targeting complex. We also found a crosslink between lysine at position 45 of CDKAL1 and at position 993 of MMS19. Furthermore, we identified crosslinks between MMS19 and numerous tubulin chains. We also tried to purify the CIA targeting complex from HHS-CIAO2B and HHS-CIAO1 before crosslinking. However, we were not able to identify any inter protein crosslinked peptides within the CIA targeting complex in these attempts.

Testing the XL-MS workflow with E. coli Ribosome – Although we demonstrated we were able to purify the CIA targeting complex and observe a few crosslinks, there are clearly improvements needed for the purpose of determining the binding interface with substrates and to further understand how the CIA targeting complex recognizes different apo-proteins. We therefore tested our XL-MS workflow using commercially purified *E. coli* ribosome. We determined the optimal crosslinking condition again by titrating with different concentrations of DSS at different temperatures (25 or 37°C) for different durations (15 or 30 minutes) (Fig. 3-2A). The ribosome was crosslinked with 4-fold molar access of DSS at 37°C for 30 minutes before processed for bottom-up proteomic analysis. We were able to detect 320 crosslinked peptide pairs (Fig. 3-2B). When we mapped the crosslinked peptides to a solved structure of *E.coli* ribosome (PDB: 5U9F), most of the C_α - C_α distances for mapped pairs fell close to 13Å, similar to 11.4Å which is the spacer arm length of DSS. 50S ribosomal proteins mostly linked to other proteins in the large ribosomal subunit, while 30S ribosomal proteins grouped with

other proteins in the small ribosomal subunit (Fig. 3-2B). These observations together suggested that our current XL-MS workflow can reliably determine connectivity of proteins in a complex and to map binding interfaces. When the ribosome was crosslinked with 4-fold molar access of DSS at 25°C for 15 minutes, we noticed that many monomeric protein bands already faded (Fig. 3-2A). We therefore tested whether crosslinking the ribosome at 25°C for 15 minutes would give comparable result as crosslinking at 37°C for 30 minutes. We were able to identify only 12 crosslinked peptides and none of them were inter-molecule crosslinked. In the cases where we cannot detect the formation of crosslinked complexes by gel electrophoresis, determining the optimal concentration for crosslinking by the disappearance of certain monomeric bands could be impractical. Lastly, we tested whether we could crosslink the ribosomes with 1-ethyl-3-[3-dimethylaminopropyl] carbodiimide hydrochloride (EDC) and detect the crosslinked peptide pairs. We analyzed the peptide mixtures digested from EDC crosslinked *E.coli* ribosome and we were able to detect 37 peptide pairs (Fig. 3-2D). The binding regions revealed by crosslinking with EDC and DSS were similar. For example, lysine at position 70 of RL31 was found linked with glutamate 24 of RS19 by EDC while it was connected with lysine at position 17 and 28 of RS19 by DSS. The C_α - C_α distances for mapped peptides were distinctly shorter than the ones crosslinked by DSS (Fig. 3-2E). Most pairs had a C_α - C_α distance around 5Å, which is consistent with EDC being a zero-length crosslinking agent.

Discussion

Given its high throughput and capability for mapping binding interfaces, crosslinking mass spectrometry (XL-MS) is a powerful tool to investigate the

architecture of the CIA targeting complex and mechanistic insights for substrate recognition. We were able to purify the CIA targeting complex with substrates using the tandem purification of Strep-Tactin Sepharose followed by Ni-NTA. We crosslinked the purified complex and were able to detect crosslinking between CIAO2B and the C-terminus of MMS19. This observation was in agreement with the recently solved structure of the CIA targeting complex.[11] We found that the N-terminus of CIAO2B is linked to lysine at position 1002, 1007, 1008, and 1013 of MMS19. We measured the distances from these linked lysines of MMS19 to proline at position 2 of the drosophila CIAO2B that aligned with glycine 9 in human CIAO2B. The distances ranged from 40 to 53Å, violating the crosslinking range of DSS. This either resulted from the longer N-terminus of human CIAO2B or indicated that the N-terminus of CIAO2B is flexible. In addition, we also found that CDKAL1 crosslinked with the lysine at position 993 of MMS19. The structural study suggested that MMS19 contacted with two prototypical CIA substrates, primase and DNA2 both at its N-terminus site and through CIAO2B and CIAO1 at its C-terminus.[11] It is possible that nearby residues of Lys 45 on CDKAL1 were in contact with CIAO1, which resulted in this crosslinking between Lys 45 of CDKAL1 and Lys 993 of MMS19. However, we still do not know whether CDKAL1 also directly binds to the N-terminus site of MMS19. In fact, we did not see any crosslinks containing the N-terminus end of MMS19. Lysine at position 292 of MMS19 is the closest to its N-terminus among all the mono-linked lysines, indicating that the N-terminal side of MMS19 may not be accessible to DSS. Using different crosslinkers aside from DSS could potentially provide a solution to characterize the interactions at the N-terminus of MMS19.

The XL-MS experiments of the *E.coli* ribosome confirmed the importance of crosslinking efficiency for successful identification of crosslinked peptides, which should be improved on crosslinking the CIA targeting complex in the future. Regardless, our XL-MS workflow can be used to study connections within protein complexes.

Experimental Procedures

Purification of the CIA Targeting Complex

Cell line expressing His6-HA-StrepII tagged MMS19, CIAO2B or CIAO1 was generated from the Flp-In™ T-REx™ 293. Twenty 150mm plates of cells were cultured in Dulbecco's Modified Eagle's Medium (Gibco™ 11960-044) supplemented with 10% fetal bovine serum (Gemini Bio-products Foundation B™ 900-208), 2mM L-Glutamine (Gibco™ 25030-081) and 1X Antibiotic-Antimycotic (Gibco™ 15240-062) at 37°C. Cells were treated with 1µg/ml doxycycline (Fisher Bioreagents #BP26535) for about 24 hours to induce protein expression. Harvested cells were lysed with lysis buffer (25mM HEPES pH 7.5, 150mM KCl, 1mM DTT, 0.1% NP-40, 5% glycerol, 1mM AEBSF, 1ug/ml leupeptin, 1ug/ml pepstatin, 1X SimpleStop2 phosphatase inhibitor, 1uM avidin) by sonication and centrifuged for 15000 RPM for 30 minutes to remove debris. Cleared lysate were loaded onto pre-equilibrated Strep-Tactin Sepharose (IBA BioTagnology GmbH). Strep-Tactin resin was washed with buffer P (25mM HEPES pH 7.5, 150mM KCl, 0.1% NP-40, 5% glycerol) before protein complexes were eluted with buffer X (25mM HEPES pH 7.5, 150mM KCl, 5% glycerol) containing 2mM biotin. Eluted proteins were incubated with pre-equilibrated Ni-NTA for 1 hour at 4°C (ThermoFisher), washed with buffer X, and left on bead for further crosslinking.

Crosslinking of Purified Protein Complexes

A portion of purified CIA targeting complexes were titrated to determine the optimal concentration of DSS for XL-MS, and the remaining were crosslinked with the optimal concentration of the isotopically coded DSS (Creative Molecules, Inc.; d_0: d_{12} = 1:1) at 37°C, 1000RPM for 30 minutes. Reactions were quenched with the addition of NH_4HCO_3 to a final concentration of 100mM. Ni-NTA bound to the crosslinked proteins were centrifuged. Supernatants were removed and beads were resuspended in 8M urea for further processing. *E. coli* ribosome (NEB #P0763S) was diluted to 1mg/ml with buffer X (25mM HEPES pH 7.5, 150mM KCl, 5% glycerol) containing 10mM $MgCl_2$ before crosslinking. Diluted ribosomes were crosslinked with either DSS or EDC. For DSS crosslinking, 50µg of ribosome reacted with 1mM linker at either 25°C for 15 minutes or 37°C for 30 minutes. For EDC crosslinking, 4mM EDC and 8mM sulfo-N-hydroxysuccinimide (sulfo-NHS) were added to 50µg of ribosome and the reaction was carried for 1 hour at 25°C. The reaction was then quenched by the addition of DTT and hydroxylamine. Crosslinked ribosomes were precipitated and washed by cold acetone and resuspended in 8M urea for further processing.

Proteomic Characterization of Cross-linked Peptides

The crosslinked proteins were reduced, alkylated, tryptic digested, and desalted for analysis by LC/MS using a data-dependent acquisition scheme. Detailed information on sample preparation and instrument setup can be found in Experimental Procedures of Chapter 2.

Identifications and Visualization of Cross-linked Peptides

Search for cross-linked peptides was conducted with pLink2 (version 2.3.9).[12] Databases for searching crosslinked peptides were generated from protein

identifications of linear peptides done by MaxQuant (2.0.3.0).[13] Spectra were searched with a precursor tolerance of 10ppm and a fragment tolerance of 20ppm. Peptides contain fixed carbamidomethyl modification on cysteines and variable methionine oxidation and protein N-terminus acetylation. Digestion was specific for trypsin with a maximum of 3 missed cleavages. Peptides with a mass of 600 to 6000 Da and a length of 6 to 60 amino acids were considered. False detection rates (FDRs) were estimated separately for cross-linked spectra, loop-linked spectra, and mono-linked spectra. FDR cut off was set at 5% at the peptide spectrum match (PSM) level. Cross-linked peptides were visualized with xiView.[14]

Reference

1. Beinert, H., Holm, R. H. & Munck, E. Iron-Sulfur Clusters: Nature's Modular, Multipurpose Structures. *Science (80-.).* **277**, 653–659 (1997).
2. Netz, D. J. A., Mascarenhas, J., Stehling, O., Pierik, A. J. & Lill, R. Maturation of cytosolic and nuclear iron-sulfur proteins. *Trends Cell Biol.* **24**, 303–312 (2014).
3. Stehling, O. *et al.* MMS19 Assembles Iron-Sulfur Proteins Required for DNA Metabolism and Genomic Integrity. *Science (80-.).* **337**, 195–199 (2012).
4. Gari, K. *et al.* MMS19 Links Cytoplasmic Iron-Sulfur Cluster Assembly to DNA Metabolism. **3801**, 2011–2013 (2012).
5. Stehling, O. *et al.* Human CIA2A-FAM96A and CIA2B-FAM96B integrate iron homeostasis and maturation of different subsets of cytosolic-nuclear iron-sulfur proteins. *Cell Metab.* **18**, 187–198 (2013).
6. Ben-Shimon, L. *et al.* Fe-S cluster coordination of the chromokinesin KIF4A alters its sub-cellular localization during mitosis. *J. Cell Sci.* (2018) doi:10.1242/jcs.211433.
7. Wang, H. *et al.* FBXL5 Regulates IRP2 Stability in Iron Homeostasis via an Oxygen-Responsive [2Fe2S] Cluster. *Mol. Cell* **78**, 31-41.e5 (2020).
8. Van Wietmarschen, N., Moradian, A., Morin, G. B., Lansdorp, P. M. & Uringa, E. J. The mammalian proteins MMS19, MIP18, and ANT2 are involved in cytoplasmic iron-sulfur cluster protein assembly. *J. Biol. Chem.* **287**, 43351–43358 (2012).
9. Seki, M., Takeda, Y., Iwai, K. & Tanaka, K. IOP1 protein is an external component of the human cytosolic iron-sulfur cluster assembly (CIA) machinery and functions in the MMS19 protein-dependent CIA pathway. *J. Biol. Chem.* **288**, 16680–16689

(2013).

10. Vo, A. *et al.* Identifying the Protein Interactions of the Cytosolic Iron-Sulfur Cluster Targeting Complex Essential for Its Assembly and Recognition of Apo-Targets. *Biochemistry* **57**, 2349–2358 (2018).
11. Kassube, S. A. & Thomä, N. H. Structural insights into Fe–S protein biogenesis by the CIA targeting complex. *Nat. Struct. Mol. Biol.* **27**, 735–742 (2020).
12. Chen, Z. L. *et al.* A high-speed search engine pLink 2 with systematic evaluation for proteome-scale identification of cross-linked peptides. *Nat. Commun.* **10**, (2019).
13. Tyanova, S., Temu, T. & Cox, J. The MaxQuant computational platform for mass spectrometry-based shotgun proteomics. *Nat. Protoc.* **11**, 2301–2319 (2016).
14. Graham, M., Combe, C., Kolbowski, L. & Rappsilber, J. XiView: A common platform for the downstream analysis of Crosslinking Mass Spectrometry data. *bioRxiv* (2019) doi:10.1101/561829.

Figures and figure legends

Figure 3-1. XL-MS of the CIA targeting complex

(A) This workflow was used for studying the architecture of the CIA targeting complex by XL-MS. His6-HA-StrepII (HHS) tagged MMS19 was expressed in HEK293 cells. HHS-MMS19 and associated proteins were purified using a tandem purification of Strep-Tactin purification of StrepII tagged proteins followed by Nickel purification of His6 tagged proteins. Purified complexes were crosslinked with a bifunctional crosslinker, in this case, disuccinimidyl suberate (DSS). Crosslinked proteins were digested with trypsin yielding inter-molecular crosslinked peptides, intra-molecular crosslinked peptides, loop-linked peptides, mono-linked peptides and a vast majority of non-crosslinked/regular peptides. Peptides were analyzed by reversed phase liquid chromatography coupled with mass spectrometer (LC/MS). Data of two technical replicates were acquired. Spectra generated were searched to identify cross-linked peptides. The identified crosslinked peptides were mapped back to proteins, inferring regions of interactions.

(B) HHS-MMS19 and coeluted proteins, without crosslinking, were analyzed by LC/MS. The search was carried with MaxQuant and results were filtered at 1% FDR at both PSM and protein level. A database constructed from all proteins identified in this linear peptide search was generated for crosslinked peptide search. The iBAQ values were calculated by MaxQuant combining the values of two technical replicates. The table includes nine proteins with the highest abundance ranked by the iBAQ value.

(C) The optimal concentration of DSS were determined by titrating the protein mixture with different molar excess of DSS. The samples from the titration were analyzed by gel

electrophoresis and visualized by silver staining. The concentration was selected at which we first saw the depletion of monomeric HHS-MMS19.

(D) The crosslinked peptides were searched with pLink2 and filtered with 5% FDR at PSM level. Only peptide pairs containing components of the CIA targeting complex were visualized by xiView. Inter-molecular crosslinks are colored in green, and intra-molecular links are colored in purple. Dashed lines indicate ambiguous results.

Figure 3-1. XL-MS of MMS19 with associated proteins

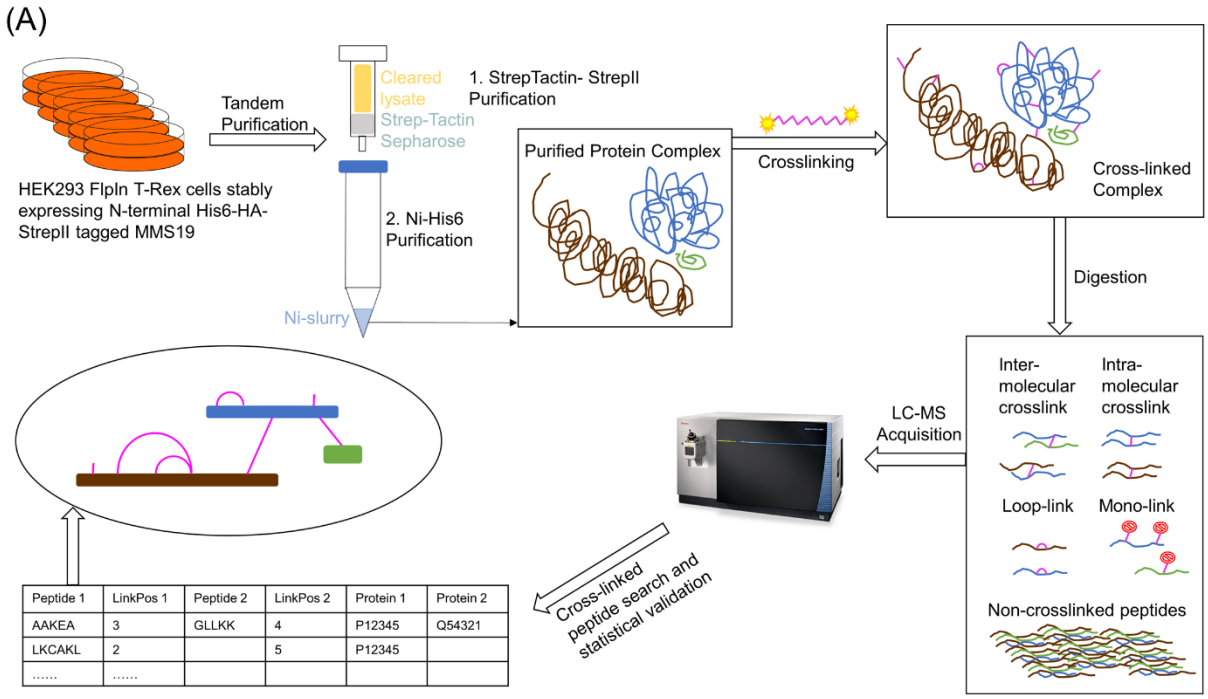

(B)

Protein	iBAQ
MMS19	9.541E+09
CIAO2B	8.943E+09
CIAO1	4.835E+09
TUBA1C	3.251E+09
TUBB4B	2.384E+09
PRIM2	2.037E+09
TUBB	1.402E+09
CDKAL1	1.284E+09
PRIM1	1.280E+09

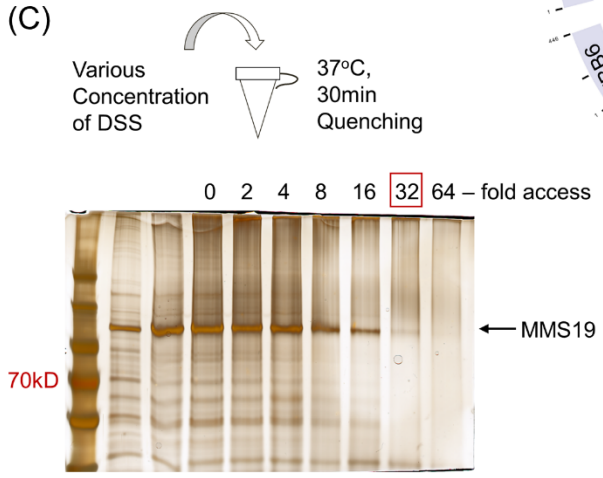

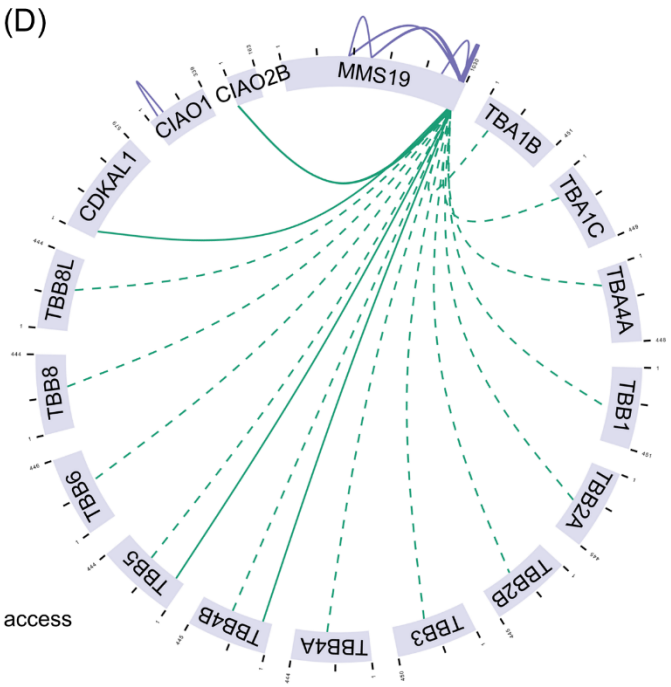

Figure 3-2. XL-MS workflow test with purified *E.coli* ribosome

(A) The *E.coli* ribosome at 1mg/ml was titrated with different concentrations of DSS at different temperatures for different durations to determine the optimal condition for crosslinking. 4X molar excess of DSS corresponded to a final DSS concentration of 1mM. The samples from the titration were analyzed by gel electrophoresis and visualized by silver staining. Red arrows point to proteins that were crosslinked and the blue arrow points to a complex formed during the crosslinking.

(B) 50µg of *E.coli* ribosome was crosslinked with 1mM DSS at 37°C for 30 minutes. Crosslinked proteins were tryptic digested and analyzed by LC/MS. The crosslinked peptides were searched with pLink2 and filtered with 5% FDR at PSM level. All the inter-molecular (green) and intra-molecular (purple) crosslinked peptides were visualized by xiView. 30S ribosomal proteins were colored in navy and 50S ribosomal proteins were colored in red.

(C) The histogram was generated with xiView showing the distribution of C_α - C_α distances of crosslinked peptide pairs that could be mapped back to a structure (PDB: 5U9F). Counts of inter-molecular (green) and intra-molecular (purple) crosslinked peptides, as well as random distances (black) were plotted.

(D) 50µg of *E.coli* ribosome was crosslinked with 4mM EDC and 8mM sulfo-NHS for 1 hour at 25°C. Crosslinked proteins were tryptic digested and analyzed by LC/MS. pLink2 was used for identifying crosslinked peptides and PSMs were filtered at 5% FDR. xiView was used to present all the filtered inter-molecular (green) and intra-molecular (purple) crosslinked peptides. 30S ribosomal proteins were in navy and 50S ribosomal proteins were in red. Dashed lines suggest that the results are ambiguous.

(E) The distribution of C_α - C_α distances of crosslinked peptide pairs in the structure (PDB: 5U9F). This histogram was prepared with xiView. Counts of inter-molecular (green) and intra-molecular (purple) crosslinked peptides, as well as random distances (black) were plotted.

Figure 3-2. XL-MS workflow test with purified *E.coli* ribosome

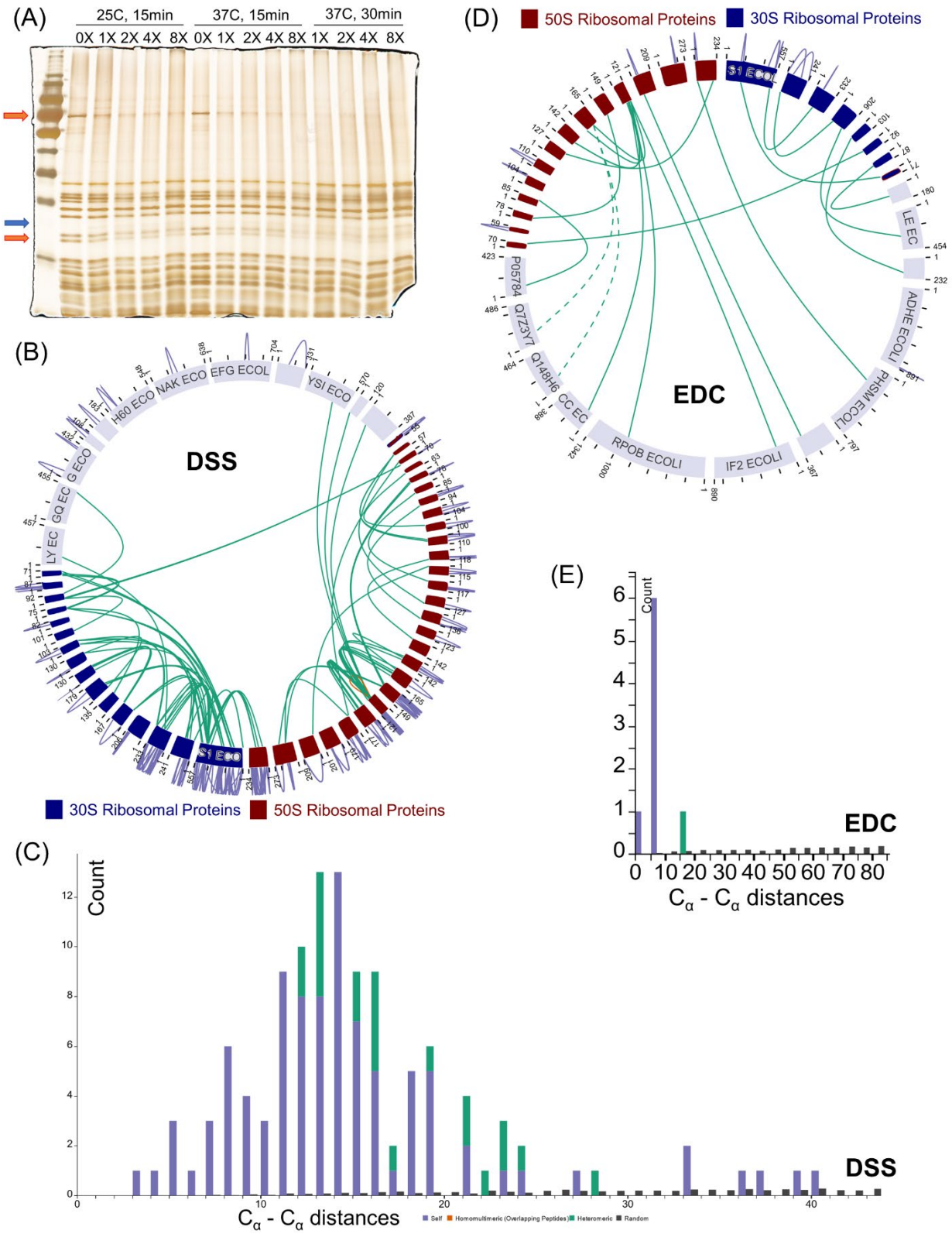

CONCLUSIONS

The reorganization of CIA machineries is central for the precise control of Fe-S protein maturation under different cellular environments. Our data demonstrate the potential formation of CIA metabolons composed of the CIA scaffold complex, CIAO3, the CIA targeting complex and CIA substrates. Furthermore, our results illustrate that the integration of CIAO3 into CIA machineries, which is regulated by environmental stimuli, requires proper Fe-S cluster incorporation into CIAO3. The discovery that CIAO3 is associated with multiple CIA substrates further supports the presence of CIA metabolons. Strikingly, these interactions are enhanced in CIAO3 mutants even with diminished interactions with the CIA targeting complex. One explanation for this observation is that CIAO3 can also form complexes with substrates in the absence of the CIA targeting complex. Alternatively, it is also possible that there are multiple forms of complexes containing CIAO3 and the CIA targeting complex, including those with and without substrates. While CIAO3 mutants may not integrate into majority of these complexes, they may be trapped in the complexes with substrates. Our study also raises a question on the source of the Fe-S clusters in CIAO3. In the current model, a [4Fe-4S] cluster is first assembled on the CIA scaffold complex and then transferred to CIAO3. However, CIAO3 mutants that are incapable to bind the scaffold complex still bear Fe-S clusters. A recent study demonstrated that a [4Fe-4S] cluster can be assembled *in vitro* on NUBP1 by reductive coupling in the presence of glutathione with the [2Fe-2S] clusters being delivered by GLRX3.[1] In the targeted proteomic characterization of CIAO3 associated protein complexes, we also detected GLRX3, raising the possibility that the [4Fe-4S] clusters in CIAO3 may be assembled *de novo* from reductive coupling of [2Fe-2S], with NUBP1/2 playing an unknown regulatory role

in Fe-S cluster binding of CIAO3, without engaging in direct cluster transfer. Additional chaperone proteins, for example HSC20, have been demonstrated to facilitate Fe-S cluster incorporation into both CIA components and CIA substrates.[2] It remains a possibility that CIAO3 maturation is mediated by either HSC20 or another yet unidentified chaperone protein.

Although our study provides evidence of iron-regulated assembly of the CIA machineries, further details on the reorganization of CIA machineries are yet to be discovered. XL-MS has demonstrated promising outcomes in probing conformation changes of protein complexes.[3] We show that we are able to obtain purified CIA targeting complex and detect crosslinked peptides within purified complexes. We anticipate that using XL-MS to investigate CIA machineries under different cellular environments will provide insightful details on how these proteins orchestrate to precisely control the Fe-S protein maturation.

Reference

1. Camponeschi, F. *et al.* GLRX3 Acts as a [2Fe-2S] Cluster Chaperone in the Cytosolic Iron-Sulfur Assembly Machinery Transferring [2Fe-2S] Clusters to NUBP1. *J. Am. Chem. Soc.* **142**, 10794–10805 (2020).
2. Kim, K. S., Maio, N., Singh, A. & Rouault, T. A. Cytosolic HSC20 integrates de novo iron-sulfur cluster biogenesis with the CIAO1-mediated transfer to recipients. *Hum. Mol. Genet.* **27**, 837–852 (2018).
3. Graziadei, A. & Rappsilber, J. Leveraging crosslinking mass spectrometry in structural and cell biology. *Structure* **30**, 37–54 (2022).